© *Proc. Indian natn. Sci. Acad.*, 51, A, No. 1, 1985, pp. 211–255.
Printed in India.

RADIATION PROCESSING OF SURFACES : APPLICATIONS OF CONVERSION ELECTRON MÖSSBAUER SPECTROSCOPY*

S B ÖGALE, S V GHAISAS, S M KANETKAR

Department of Physics, University of Poona, Pune 411 007

and

V. G. BHIDE

School of Energy Studies, University of Poona, Pune 411 007

Recent advances in the modification of surface layers using techniques such as ion implantation, ion beam mixing, laser annealing and alloying, electron beam annealing are discussed. These techniques have distinct advantages over conventional methods such as thermal diffusion, tinning, boriding etc, inasmuch as, with these techniques it is possible to modify surface layers to the required specifications without affecting the bulk in any way. All these techniques are non-equilibrium in nature and can give rise to exotic metastable phases, in which Hume Rothery rules are considerably relaxed. Some of the applications of the surfaces modified using these techniques are also described.

Various attempts made to characterise the modified surface layers using techniques such as Rutherford Backscattering, low angle X-ray diffraction, resistivity measurements are mentioned. With these methods, it is not possible to characterise the modified surfaces to the atomistic details and to obtain information on the mechanism of the process of surface modification. In this context, the utility of Mössbauer spectroscopy in scattering mode is brought out and the use of the technique of conversion electron Mössbauer spectroscopy in characterising the surface layers is described in details.

Some of the recent experiments on the application of Conversion Electron Mössbauer Spectroscopy for the characterization of surfaces modified using directed energy processing techniques are discussed. A few other applications of Conversion Electron Mössbauer Spectroscopy for the study of surface reactions, interfaces etc. are also described.

Key Words : Radiation Process; Mössbauer Spectroscopy; XRD and CEMS

1. INTRODUCTION

IN recent years, there has been an enormous growth of research activity in the field of material science. The major attention of this activity is focussed on the question of obtaining material surfaces tailored to the required specifications[1–4]. The conventional technique of equilibrium thermal treatment either for alloying, annealing or impurity diffusion can not offer a useful solution to this problem because of three reasons[4]; (i) In the thermal case there are no parameters to control except the temperature and treatment—time, (ii) the equilibrium thermal treat-

*Paper presented at the Symposium on Physics and Chemistry of Surfaces held at INSA, New Delhi from September 28–30, 1984.

ment can only yield stable phases of materials and, metastable phases having newer features can not be synthesized (By using non-equlibrium thermal methods such as splat-quenching[5], one can obtain metastable phases of different materials and composites; but these methods are not useful in modifying the properties of a given material); and (iii) the thermal treatment cannot be region selective within a small volume of the sample and as such, by using this method it is not possible to modify the properties of a given material differently in different distributed regions within a small volume. Hence, during the past decade there has been a considerable growth of interest in the use of the radiation processing methods to tailor the properties of solid surfaces to the desired specifications[6–11].

Considerable experimental work has already been done in this research area so as to understand the physical processes which can occur when radiation of a specific type is incident on the material surface. In most of these studies the techniques of Rutherford Backscattering (RBS), X-ray diffraction (XRD) resistivity measurements etc. have been employed and valuable information regarding the structural and chemical properties of processed layers has been obtained. Yet a need is felt for additional data[9], especially on the atomistic aspects of the beam induced processes, so as to reveal the finer details regarding the nature and properties of the new materials which can be synthesized by using the beam processing techniques. Amongst the characterization techniques which can directly address to the atomic level details, the technique of Mössbauer spectroscopy[12,13] has a special place because, this technique can, in a single measurement, bring out an information regarding the structural, chemical, electrical a well as magnetic properties of materials along with a valuable data on the defect complexes and their symmetries. Also, this technique being non-destructive in nature, it does not forbid the use of the other characterization concepts for studying the same material; thus a coherent picture regarding state of the solid can be obtained without difficulty. Mössbauer spectroscopy provides a number of windows such as isomer shift, quadrupole splitting, magnetic dipole interaction, Lamb Mössbauer factor etc. through which one can obtain an extremely useful information about the nature of chemical environment, symmetry of the neighbours, magnetic field at the nuclear site, dynamics of the Mössbauer atom etc. Yet, the use of this technique requires presence of suitable isotopes of elements which can serve as source and absorber nuclei in a Mössbauer experiment, and as such this technique can not be conveniently applied to the studies of arbitrarily chosen material system. However, by making an appropriate choice of a representative Mössbauer system, the physics of the non-Mössbauer accessible materials can also be studied by this method.

In the following section (Section II) we have briefly discussed some important radiation processing techniques which are of current interest, and in Section III, the elements of the theory of Mössbauer effect have been discussed, alongwith the information regarding the experimental systems used for Mössbauer measurements in transmission, scattering and conversion electron modes[14]. In Section IV, a number of examples of the use of Mössbauer spectroscopy in characterizing radiation processed surfaces have been given.

2. Radiation Processing of Surface Layers

As mentioned earlier several radiation processing techniques have been developed over the past decade to tailor the properties of material surfaces to the desired specifications. The prominent ones among these are the techniques of ion implantation[6–8], ion beam mixing[9], laser treatment[10], electron beam treatment[3,11] etc. In the following, these techniques have been briefly introduced and their potentialities for rendering a desired surface modification have been brought out.

2.1. *Ion Implantation*

This method of surface modification is based on the bombardment of solid surfaces with selected ionic species having energy in the range of a few tens to a few hundreds of KeV[6–8]. This is a high vacuum (10^{-6} Torr) process which offers a possibiliy of obtaining a specific dopant distribution in the submicron region below the solid surface by controlling the ion energy, target temperature, orientation of the target structure with reference to the ion direction etc. Various physical processes can occur when an energetic ion hits the solid surface. Since the implantation energies used in most experiments are in the KeV range, the atoms of the solid which are displaced from their sites by the incoming ions also possess substantial energy to atomically displace other atoms on their track, leading to the formation of a 'Collision Cascade Region' which generally has a high concentration of vacancies[15]. This region is often surrounded by distributed interstitials. The cascade formation occurs over a time scale of only 10^{-13}—10^{-10} secs which renders a high non-equilibrium nature to the implantation process. The depth distribution of implanted ion concentration generally has a semi-Gaussian nature as shown in Fig. 2.1 (a). Under special circumstances wherein the ions are incident on a crystalline solid along one of its low index crystallographic directions however, anamolous range distributions can result due to ion-channelling effects (See Fig. 2.1 (b)). In the normal situations (no channelling case) the projected ion ranges (or typical penetration depths) are of the order of a few hundreds of Angstroms; while under channelled conditions the ions can penetrate as deep as a few microns.

Since ion implantation leads to a forced and transient introduction of dopants into solids, this highly non-equilibrium process can be used to surpass the limits of solid solubility allowed by the Home-Rothery rules[16] and to synthesize extended solid solutions. This aspect is especially important in the context of metals, wherein one desires to obtain newer metastable alloys with novel application potentials. In order to obtain high concentration alloys however, the process of direct implantation is not suitable because, to obtain high concentration alloys the requirement of ion dose is as high as 10^{17} — 10^{18} ions/cm^2, and at such dose values the sputtering effect[17] erodes the pre-synthesized alloy layers. Very recently it was shown by Tsaur *et al.*[18] that a simple but interesting variation of the implantation method itself can be used to synthesize concentrated metastable alloys on the surfaces of any material without the intrinsic limitation imposed by the sputtering effect in the direct implantation case. This innovation is referred to as ion beam mixing.

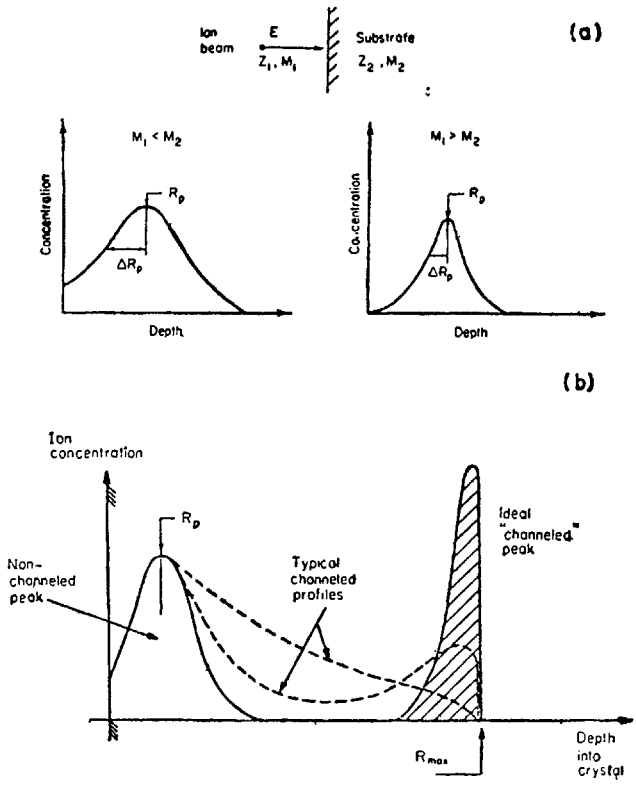

FIG. 2.1 Depth distribution of implanted ions (a) in an amorphous target (M_1 is the mass of the incident ion and M_2 is the mass of the target atom) and (b) in a single crystal under the condition in which the beam is aligned with a major crystallographic axis (channelling case).

2.2. *Ion Beam Mixing*

The principle of ion beam mixing[9,18,19] has been depicted in Fig. 2.2(a). This technique is based on the fact that one energetic ion incident on a solid surface can dynamically move nearly hundred or more of the atoms of the surface layers over many lattice distances. Hence, an ion dose of 5×10^{15} ions/cm^2 can lead to a dynamical mixing of 10^{17} to 10^{18} atoms in the surface layers of a solid. If these layers are composed of successively deposited thin films, an atomic mixing of these films can take place yielding a homogeneous high concentration alloy. Of course, for alloy formation, the energy of ions should be such that the ions cross the interface where the process of mixing begins. Generally, the energy of ions is so chosen as to yield a projected range R_p equal to the depth of the interface below the solid surface. Clearly, if one wants to synthesize thicker layers of metastable materials, then higher ion energy has to be employed. The energy can not however be far greater than a few hundred KeV because, beyond this typical energy regime (50–400 KeV) the ion-nuclear cross-section diminishes at the cost of an enhancement of the electronic excitation cross-section and efficient dynamical mixing can not take place.

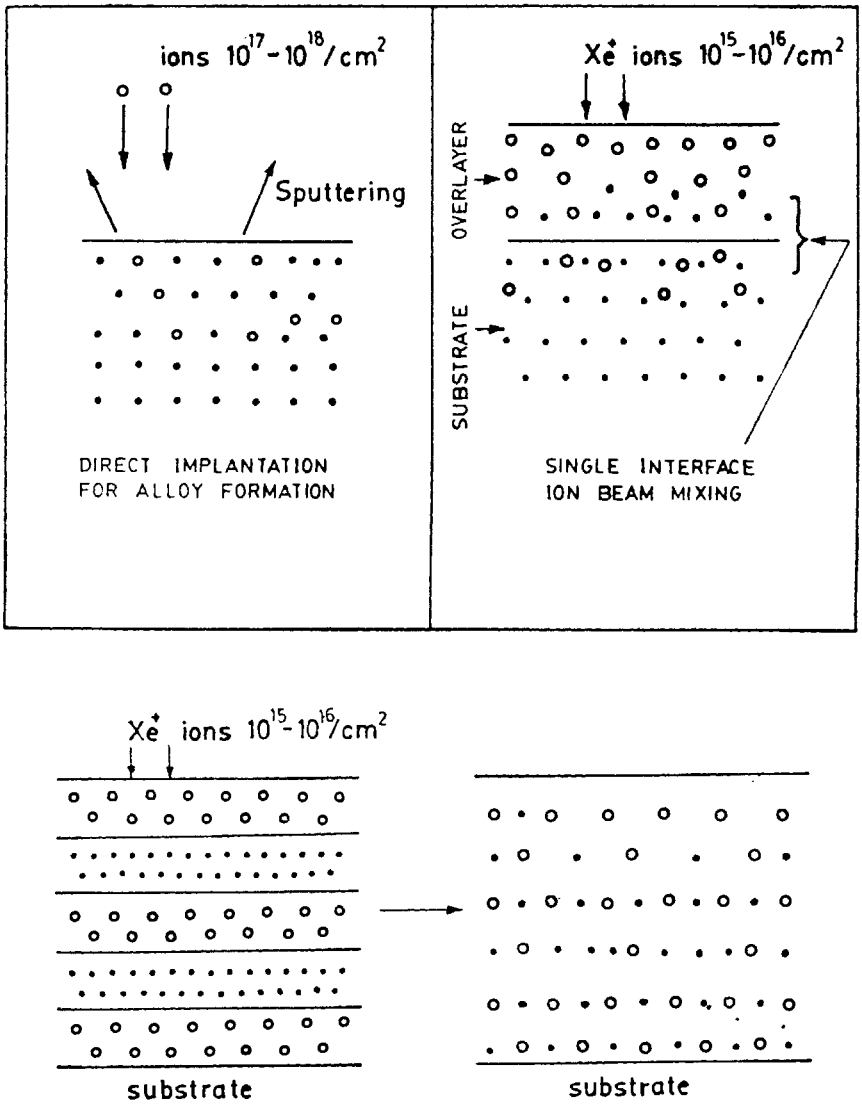

FIG. 2.2 (a) Schematic representation of ion beam mixing process when an energetic ion is incident on a thin film couple.

(b) Ion beam mixing process in the case of a multilayered structure.

It may be noted that the ion dose required to form a concentrated alloy is almost two orders of magnitude lower in the case of the ion beam mixing than that required in the direct implantation method. Hence, the sputtering limitation of the latter method is almost completely eliminate[9]. Also, in view of the small dose, the percentage of the implanted ions in the composition of the mixed alloy is extremely

small and thus, beam mixing can be carried out by using any suitable ions of chemically inert gaseous species such as Ar^+, Kr^+, Xe^+, etc, with little risk of influencing the physical properties of the alloy. This avoids the requirement of solid ion production and acceleration, intrinsic of the direct implantation method and relatively simple implantation machines can be used to carry out the alloying process. It may also be observed that since the basic process used in ion beam mixing in ion implantation itself, it preserves the most important advantage of the implantation method, viz. its highly non-equilibrium nature which can lead to novel metastable structures and compositions.

It may further be pointed out that the technique of ion beam mixing can be used effectively to tailor the composition of the mixed layer [see Fig. 2.2(b)]. This can be achieved by preparing a layered structure of alloying elements having thickness suitable to yield specific final composition and subsequently, mixing the deposited multilayered sandwich by energetic inert gas ions. In this multi-interface case, the energy of ions used to achieve mixing may be varied over a chosen range.

2.3. *Laser Treatment*

The laser treatment of materials which was initially developed to anneal the implantation induced damage can be performed by using high power lasers operating either in a 'Pulsed' mode[10,20-22] (Q-switched Ruby, Nd-YAG lasers etc.) or CW mode[23-25] (Co_2, Ar, CW Nd-YAG laser etc.). The power requirements for imparting a certain modification to the surface differ in the two cases for obvious reasons. Also, the mechanism of the modification process is substantially different in the pulsed and CW cases; and hence one may not be able to attain a specific state of the material surface by both the methods. In particular, when one uses pulsed Laser having pulse width of a few tens of nanoseconds or smaller, highly non-linear processes occur in the submicron region near the sample surface; and, structurally and compositionally metastable layers can be synthesized[11]. In view of its highly non-equilibrium nature, the pulsed laser treatment has emerged as an area of immense scientific interest in the recent years and as such, in the following discussion we have mainly concentrated upon the pulsed laser technique of material processing.

The technique of pulsed laser treatment has been found to be extremely useful in achieving the following objectives[10] : (i) Annealing of implantation induced damage; (ii) redistribution of implantation profiles; (iii) epitaxial growth of amorphous layers deposited on crystalline surfaces; and (iv) alloying of the layers of different materials[11] so as to obtain novel metastable phases of materials. The experimental process of impurity redistribution and surface annealing has been depicted in Fig. 2.3(a); while in Fig. 2.3 (b) the process of pulsed layer induced alloying has been shown. A laser pulse having a pulse width of a few nanoseconds and an energy density of a few Joules/cm^2 is generally employed in such experiments. In specific applications, such as in the formation of a glassy metal metalloid alloy, even picosecond laser pulses have been employed[24].

The pulsed laser treatment has a number of interesting and useful features which cannot be realised by using other procesing methods : (i) This technique being

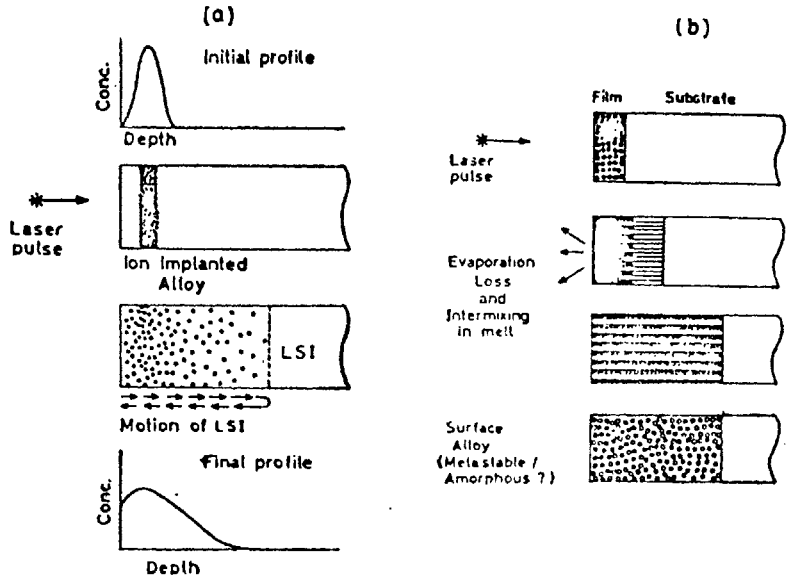

FIG. 2.3 Schematic of (a) the redistribution of implanted impurities due to the pulsed laser treatment and (b) mechanism of pulsed laser induced mixing of an overlay solute film on a substrate.

an optical processing method, it does not leave its mark on the solid-state, subsequent to the completion of the transient modification process; (ii) by focussing the optical radiation, this method can be easily rendered to be highly area selective; (iii) since the pulse duration is generally less than a few tens of nanoseconds, this process can be carried out in air without any risk of oxidizing the submicron layers (In fact, it has been shown that not more than a few monolyarers are oxidized during the extremely fast transient surface processing); (iv) this method is far more simple and quicker as compared to any other surface modification technique and as such it is easy for automation; (v) this method allows an easy control of the depth of the annealed region and also the extent of impurity redistribution by an appropriate control of the pulse parameters; (vi) since this is a highly non-equilibrium process (quenching rate 10^8–10^{10} °K/s) metastable phases can be synthesized; and (vii) the thickness of the surface layer which can be effectively modified is considerably larger (in microns) as compared to that by the other techniques such as ion implantation, ion beam mixing etc. In view of these tremendous advantages it is not surprising that the method of pulsed-laser treatment has acquired a prominent position amongst the newer and unconventional methods of material modification.

Although the experimental aspects regarding the results of the laser treatment seem to have been understood reasonably well, the physical processes occurring over the short processing time-scale appear to have many complexities which have not been clearly understood[26–28]. When the laser radiation is incident on a solid it can be absorbed by various processes; the primary channel of absorption being via the excitation of the electronic system. Thus, the pulsed laser can instantly pro-

duce a very large concentration of electrons and holes in the region of optical absorption and this electron-hole plasma can then loose energy to the lattice by generation of phonons, leading to the melting of the solid. The structural and compositional transformations may then be expected to occur in the molten phase, whose spatial and temporal development is dependent upon the absorbed laser power as well as the parameters of the meterial itself such as its specific heat, thermal diffusivity, solubility conditions in the case of the composite system etc. This model which is popularly known as the 'melting model' has been found to be adequate to explain most of the observations.

2.4. *Electron Beam Treatment*

Electron beam can also be used for processing materials both through thermal effects and through non-thermal or chemical, effects[29]. In the annealing or alloying applications, the thermal aspects of the electron beam treatment of surfaces is exploited. The electron beam processing method has certain specific advantages over the laser annealing technique : (i) In the process of laser annealing the sample undergoes significant changes in reflectivity, and as such there is a considerable uncertainty regarding the amount of energy actually absorbed by the sample. The electron beam treatment does not suffer from this drawback: (ii) Very high, steady-state values of power per unit area can be maintained in the case of electron beams by adequate emission control and the control of the focussing conditions. Also, the value of the incident power can be measured precisely bya ppropriately compensated Faraday-cup assemblies. In the case of laser beams, especially the pulsed-lasers, the determination of absolute power is an extremely complicated process. Moreover, it is difficult to obtain an areal uniformity of better than a few percent without the use of beam homogenizers which leads to considerable loss of beam energy; (iii) in the case of electron beams (used in continuous mode) a controlled scanning of the beam across the area can be performed easily by electrostatic and/or magnetic deflection methods; while in the case of the laser beams, the scanning in most cases involves mechanical motion of the target. The electron treatment, however, has a major drawback as compared to the pulsed laser treatment viz. the electron treatment systems necessarily require vacuum operation, which is not the case with pulsed-laser treatment as mentioned earlier. Yet, for its specific advantages the electron beam treatment stands out as an independent and useful alternative for material processing. The typical parameters of the electron beam, which can yield a suitable surface modification are :

Pulse duration	:	40–400 ns
Electron energy	:	5–50 KeV
Total current	:	1–50 KA
Beam diameter	:	8–10 cm
Pulse energy	:	upto 20 Joules/cm^2

Such a continuous high current electron beam can be generated by hot cathode assemblies and such beams in the scanning mode can be used for lithography, welding, annealing etc.

Apart from the techniques of ion implantation, ion beam mixing, laser treatment and electron beam treatment which have been discussed in the above paragraph, there exist a host of other techniques which are capable of modifying the material surfaces in a variety of ways. These include pulsed ion beam treatment, flash-lamp (incoherent light source) annealing, transient heat pulse treatment via resistive heating, plasma treatment etc. These techniques are still in the stage of development and we shall omit a detailed discussion concerning them in the present article. Since this article refers to the applications of Mössbauer spectroscopic technique to the study of radiation processed surfaces, we now turn our attention to some basic concepts concerning Mössbauer spectroscopy and different experimental channels available to observe this nuclear resonance absorption.

3. Mössbauer Spectroscopy

3.1 *Mössbauer Effect (Basic Considerations)*

Mössbauer effect[12–13] refers to the recoilless emission and absorption of gamma rays by atomic nuclei. In view of the high energy and hence momentum transfers associated with a gamma transition, the energy required to be spent in compensating for the recoil motion of the emitting or absorbing nuclei is high enough to disallow the realisation of any resonant exchange of gamma photons between free atomic and molecular systems. However, when a gamma-emitting or absorbing atom is strongly bonded into a solid, the recoil can be taken up by the entire solid; thus diminishing the recoil energy to a negligibly small value and making a recoilless exchange of gamma photons possible. Since the gamma rays involved in the Mössbauer effect emerge in a recoilless mode, they are characterised by a spread of energy corresponding only to the natural linewidths of the nuclear levels and hence, even minute perturbations caused to the environment experienced by the nucleus can be very sensitively reflected in the results of a Mössbauer experiment. This is especially important in the context of the studies of material systems, wherein extremely small perturbations are caused to the nuclear levels via hyperfine interactions, which represent the interactions between a nuclear property such as electric quadrupole or magnetic dipole moment and appropriate electronic and atomic properties. Since the variations in the nuclear energies caused by the changes in the structural, chemical, magnetic and electrical state of the environment of a Mössbauer nucleus can be measured with an accuracy of 1 eV in 10^{13} eV or better (e.g. in the case of Fe^{57}) by using the Mössbauer technique, this method of material characterization has found a central place in the field of material science. In a typical Mössbauer experiment [see Fig. 3.1(a)] one uses a source, which is in the form of a crystalline medium embedded with atoms having Mössbauer active gamma emitting nuclei and an absorber (which is the sample under study) containing atoms of the isotope which represents the ground state of the gamma emitting nuclei in the source medium. If the source is moved in a constant acceleration mode (so as to obtain a Doppler spread of frequencies) then the various possibilities of excitation of absorber nuclei appear as sharp dips on the scale of source velocity. By deconveluting such spectra,the nature, strength and symmetry properties of the different hyperfine interactions can be studied.

There are three main hyperfine interactions which are of great importance in the context of Mössbauer spectroscopy. These are :

i. Electric monopole interaction (e0)
ii. Magnetic dipole interaction (ml) and
iii. Electric quadrupole interaction (e2)

The first type of interaction emerges as a result of the Coulomb interaction of the nuclear charge and the S-electron density at the nucleus, and leads to a shift of the centre of gravity of the Mössbauer spectrum with reference to the zero velocity position. This interaction is referred to as 'isomer shift'. The second and third type of interactions lead to the occurrence of multiplets in the Mössbauer spectrum and such multiplets correspond to the Zeeman and quadrupole splitting of the nuclear levels. In addition to these parameters, recoilless fraction and linewidth corresponding to Mössbauer spectrum also provide very useful information regarding the

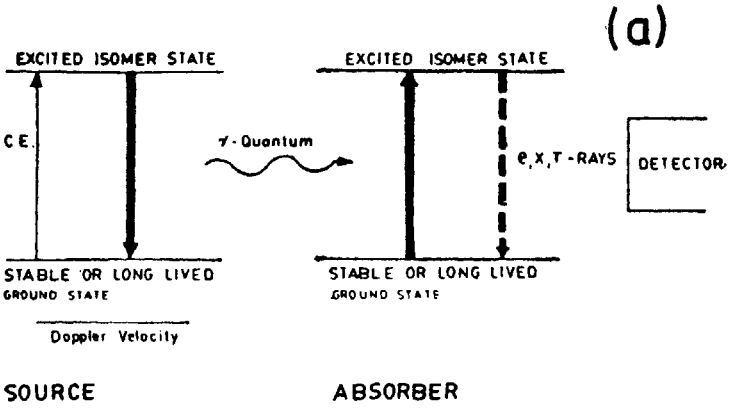

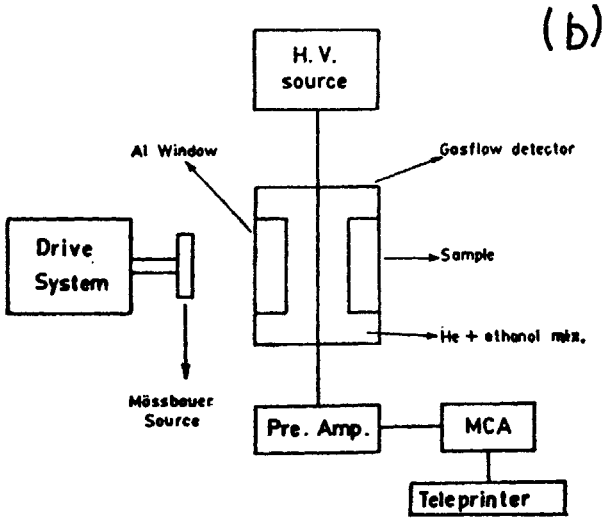

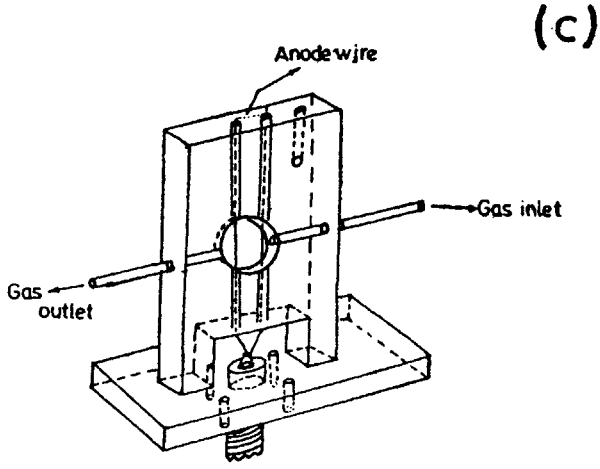

FIG. 3.1(a) Schematic representation of nuclear γ-ray resonance fluoroscence, (b) A block diagram of the experimental set-up for the Conversion Electron Mössbauer Spectroscopic studies, (c) A typical gas flow conversion electron detector.

diffusion processes of atoms, disorder in the lattice, distribution of hyperfine para meters etc. Especially, in the case of amorphous alloys, it is of interest to study the collapse of linewidth with the thermal annealing treatment so as to infer about the ensuance of atomic order, nucleation and growth of alloy phases etc.

3.2. *Scattering Mössbauer Spectroscopy*

When a γ-photon interacts with a nucleus of an atom bound in a solid matrix, a variety of phenomena can take place. In the earlier paragraphs we have discussed only the nuclear absorption process which can be studied in the Mössbauer transmission mode. Other possibilities include gamma ray scattering, de-excitation of the nuclear state formed by gamma absorption via emission of gammas, β-particles X-ray etc. or by other complex decay schemes involving the composite nuclear and electronic system. All these possibilities can be exploited to carry out some immensely interesting experiments of both the basic as well as applied nature, and a host of new information can be generated. These studies are classified under the category of 'scattering Mössbauer Spectroscopy'.

Amongst the radiations which are emitted by the absorber nucleus (Table I) subsequent to the γ-absorption, the K-shell conversion electrons have been found to be particularly suitable to perform Mössbauer studies on surfaces, interfaces and thin films; and this technique is popularly known as Conversion Electron Mössbauer Spectroscopy (CEMS)[14,30].

In the case of Iron, which is an element of considerable interest in the context of Mössbauer spectroscopy, the K-conversion electrons have an energy of 7.3 KeV, and their intensity is 79% of the total deexcitation radiation. The typical distance

TABLE 1

Type of emitted radiation	E (KeV)	Intensity	Range 'r' in Fe metal
Gamma rays	14.4	0.11	$r \sim 20\,\mu m$
K X-rays	6.3	0.28	$r \sim 20\,\mu m$
L X-rays	0.7	0.002	
K-shell conversion electrons	7.3	0.79	$10\text{ nm} \lesssim r \lesssim 400\text{ nm}$
L-shell conversion electrons	11.6	0.08	$20\text{ nm} \lesssim r \lesssim 1.3\,\mu m$
M-shell conversion electrons	14.3	0.01	$20\text{ nm} \lesssim r \lesssim 1.5\,\mu m$
K-LL Auger electrons	5.5	0.6	$7\text{ nm} \lesssim r \lesssim 200\text{ nm}$
L-MM Auger electrons	0.5	0.6	$1\text{ nm} \lesssim r \lesssim 2\text{ nm}$

Energies, intensities and ranges of photons and electrons emitted after resonant excitation of the 14.4 KeV state of ^{57} Fe (electron con0ersion coefficient $\gamma = 8.2$). Radiations emitted with energies lower than 0.5 KeV are not included.

over which these electrons loose their energy in solids is 0.25 μm. Thus, conversion electrons emitted within this distance below the surface of a solid alone can be ejected out of it, conveying the Mössbauer information. Moreover, if these electrons are detected in a proportional mode, the pulse height selection can allow a further control on spatial selectivity of the Mössbauer signal. Thus, in a sense the technique of conversion electron Mössbauer spectroscopy [Fig. 3.1(b)] is a superior mode of operation than other scattering modes so far as the surface layer characterization is concerned. Also, this method is very sensitive because of the high signal to noise ratio attainable in this case. Since internal conversion coefficient depends inversely on the excitation energy, and since the most viable Mössbauer sources (like Fe) have reasonably small γ-ray energy, the differential cross-section for γ-e scattering is comparable to and often larger than that of the γ-γ scattering. This enables one to carry out an efficient Mössbauer characterization of submicron layers below material surfaces. The CEMS technique has been considerably exploited in the studies of a variety of phenomena such as corrosion[31–33], oxidation[34–35], surface magnetism[36] ion-implantation[30–35], etc.

In a typical CEMS detector the conversion electrons emitted from the sample are detected in a gas filled proportional counter or with a channelltron, depending upon the type of information one desires to obtain. In a gas filled detector, in most cases, the entry of the conversion electron is registered irrespective of it's energy; and all the electrons with varying energies at 'on and off' resonance conditions are counted in integral manner. On the other hand, in the arrangement using channeltron, not only the entry of electron is registered but it's energy is also measured, leading to a degree of depth selectivity. This is called a Differential Conversion Electron Mössbauer Spectroscopic technique (DCEMS).

The simplest possible design of a CEMS detector is the one which makes use of an 'Anode wire between parallel plate' type of a geometry[14] [See Fig. 3.1(c)]. In

such a detector more gas multiplication occurs only in a very small region around the wire and the pulse height is independent of the direction of travel of the electron as well as the site of the primary ionisation. This leads to a reasonable energy resolution and proportionality. We have developed such a detector and an associated experimental system in our laboratory to perform CEMS studies on radiation processed surfaces.

Figure 3.2 shows a typical spectrum of an Iron foil (containing 2.2% of Fe^{57} Mössbauer isotope) obtained by using our system under the following choice of the different operating parameters :

1.	Anode voltage	=	900 volts
2.	Rate of gas flow	=	10 cc/min
3.	Distance between anode and the sample	=	0.3 cm
4.	Distance between two anode wires	=	0.5 cm
5.	Average pulse height	=	0.2 volts
6.	Ethanol temperature	=	0°C
7.	Sample and ambient temp.	=	300°K

The percentage effect exhibited by this spectrum is 12%. Recalling that this spectrum is due to the Fe^{57} atoms within a distance of 0.25 μm below the surface, this result demonstrates that a simple gas filled detector can yield a performance which is quite satisfactory for most of the room temperature Mössbauer studies on material surfaces, interfaces and thin films. In order to perform CEMS studies at low (LN_2 or Liquid He) and high (600°C) temperatures, different detector designs have to be used.

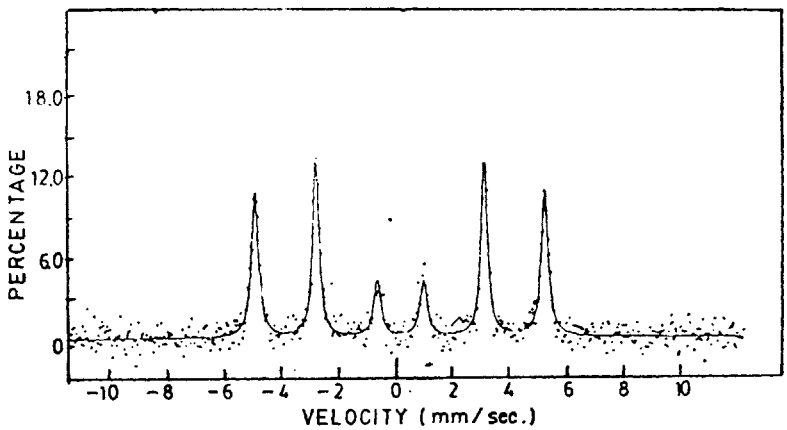

FIG. 3.2 Typical Mössbauer spectrum of iron foil surface obtained by conversion electron Mössbauer spectroscopic technique.

3.3. *Other Advances in CEMS Technique*

In all the earlier considerations we have restricted ourselves only to the absorber experiments in Mössbauer spectroscopy. Another interesting possibility of carrying out Mössbauer studies on material systems is afforded by the source experiments, which can bring out very useful information concerning dynamical processes such as diffusion. In order to carry out source experiments on surface layers a novel design concept has been suggested by Mullen *et al.*[37] His CEMS detector, which is referred to as a MICE (Micro-foil Conversion Electron) detector, consists of a series of 1 mil. diameter tungsten wire anodes alternated with cathodes of Fe^{57} enriched stainless steel foils having a thickness of $\sim$ 3000Å. The counter is operated as a flow counter using a premixed-helium and 8% methane as the gas mixture. The operating voltage of one counter is typically 800V. The signal to noise ratio of such a detector can be enhanced by either applying upper and lower discriminators or by utilizing thin sheets of lucite to selectively filter the 6.3 KeV X-rays. In order to bring out the advantages offered by the MICE detector, we have reproduced in Fig. 3.3 the results of Mullen *et al.* on the comparison of the MICE and the proportional

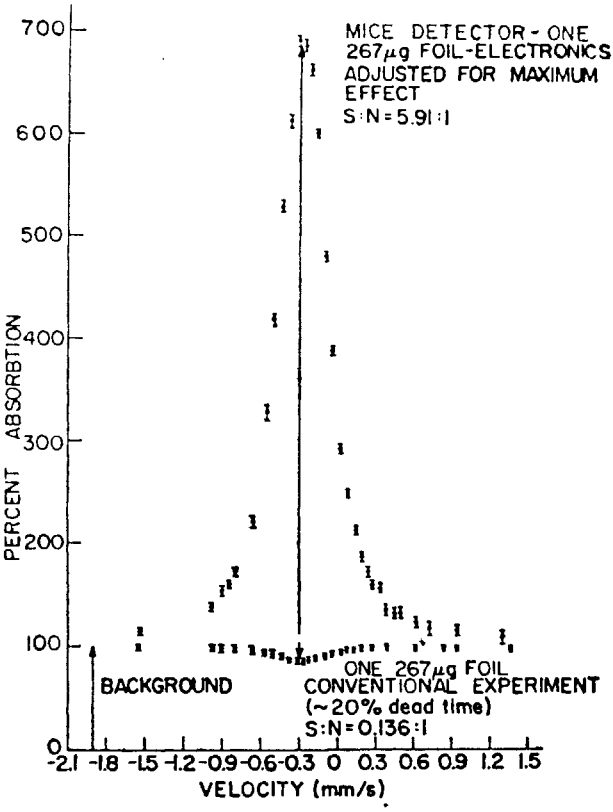

FIG. 3.3 A large 'f' experiment, illustrating the signal to noise enhancement of the MICE detector compared to a proportional counter used in transmission experiment.

detectors. It is clearly seen that the MICE detector enhances the signal to noise ratio by a factor of over 40 in this case, while the differences between the on-resonance and off-resonance count rates is only a factor of 2 less for the MICE detector as compared to the proportional detector. Thus, the MICE detector offers newer possibilities of performing Mössbauer characterization of materials.

Another important aspect of the surface Mössbauer Spectroscopy on which work is presently in progress is the depth selective CEMS technique. Depth selective CEMS requires analysis of electron spectra with a good energy resolution. These experiments have to be performed using electron spectrometers with high luminosity and high transmission. In spite of many serious attempts made to achieve these aims however, it has not been possible to enhance the depth resolution of the CEMS technique to such a value as to allow a reasonably good determination of interface composition profiles, distribution of implanted ions in solids etc. Thus, further progress in this direction is necessary.

Finally, a reference may be made to an interesting work by Tyliszczak *et al*[38], who have demonstrated that good quality Mössbauer spectra can be recorded even with resonant electrons at an energy as low as 10 eV or below. With improvement of such a technique interesting new possibilities of investigations in the field of surface science can be foreseen.

4. Applications of Conversion Electron Mössbauer Spectroscopy(CEMS) to the Studies of Radiation Processed Solids

The CEMS technique was first applied to the study of ion implantation[39] in 1975 and since then, this method of Mössbauer characterization has been successfully applied to a number of useful studies on radiation processed solids. In what follows, we have given illustrative examples of the applications of the CEMS technique to the studies of ion implantation, ion beam mixing and laser treatment.

4.1 *Ion Implantation : CEMS Studies*

Sawicka *et al.*[30] have studied the Fe^{57} implanted Al, Si, Ge and diamond samples by using the CEMS technique. In the case of aluminium host these authors have studied the effects of Fe^{57} implantation[40] over an ion dose range of 10^{14} ions/cm^2 to 2×10^{17} ions/cm^2. The maximum average ion concentration in aluminium which has been attained is $\sim 30\%$, which is far above the solid solubility limit of iron in aluminium (0.001% at room temperature and 0.025% at 650°C). Some results of CEMS measurements on Fe^{57} implanted in aluminium are given in Fig. 4.1. At iron concentrations smaller than 5% the spectra are composed of a singlet and a quadrupole split doublet. The single line can be attributed to iron monomers, while the doublet to higher iron associations (especially dimers[41]). As the average iron concentration is raised up to 5% the contribution of the single line decreases while that of the doublet increases systematically. The values of isomer shift corresponding to the two contributions show that the S-electron density at Fe-nucleus

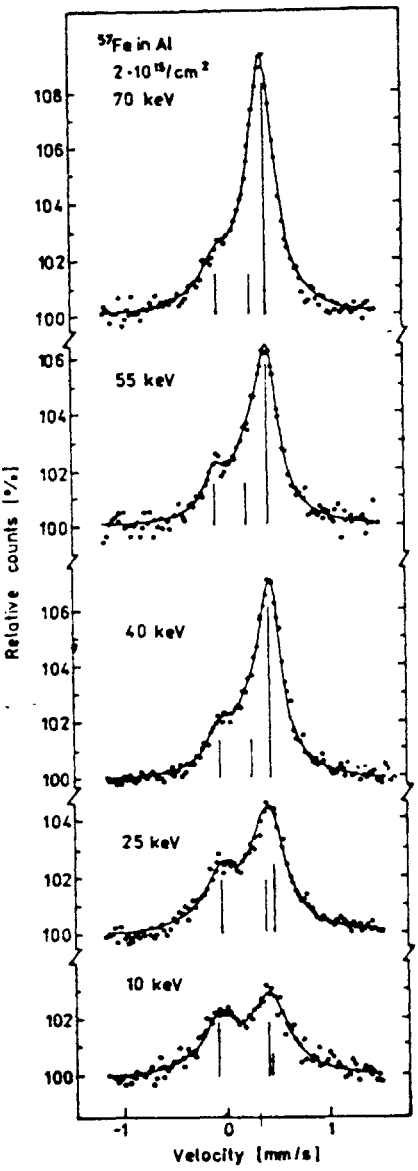

FIG. 4.1 Variation of CEM Spectra of Fe^{57} implanted in Al with ion energy and therefore, with concentration of implants ($\bar{x} = 0.5\%$, 0.6%, 0.9%, 1.1% and 2.1% respectively). A single line is due to iron monomers and a doublet is due to iron dimers.

is larger in iron dimers than in the monomers. In this case the CEMS technique has also revealed that the iron aggregation process is enhanced both by implantation at high doses (leading to high defect concentrations) and by thermal treatment. In fact, the fast quenching nature of ion implantation process has a very significant

contribution which can be seen from the fact that at dose values which are not high enough to lead to the formation of large iron clusters and yet high enough to surpass the limits of solid solubility, the contribution of iron monomers (non associations) does appear in the CEM spectra. These and other results on metallic hosts implanted with Fe^{57} ions reveal that the relative sizes of iron and the host atom play a significant role in deciding the final site of the implanted atoms in the host structure[30]. The Fe^{57} ions implanted in Fe, Co, Ni, Ru, Rh, Pd, Re, Os, Ir and Pt matrices indicate a good substitution of the host atoms and no contribution of dimers. On the other hand, Fe^{57} implantation in V, Cr, Rg, Mo and Ta (which incidently are bcc lattices) leads to the formation of a state in which monomers and dimers coexist. The Cracow group has also studied Fe^{57} implantation effects in silicon[42] and germanium[43] over a dose range between 5×10^{14} to 5×10^{16} ions/cm^2 and has obtained a very useful information about the implantation process.

Apart from the above mentioned basic studies on the physical processes associated with ion implantation, the CEMS technique has also been used to perform studies of applied nature in the same field. Baumvol has studied the influence of tin implantation on the oxidation of iron[34]. He has studied the influence of the implantation of Sn^+ ions over a does range between 5×10^{15} ions/cm^2 and 5×10^{16} ions/cm^2 on the oxidation of iron at the temperatures between 300°C to 500°C. It has been shown that the implantation of Sn^+ reduces the oxidation rate constant of iron upto a factor of ten, at all the experimental temperatures. Baumvol has used the Rutherford Backscattering, SEM (Scanning Electron Microscopy) and CEMS techniques to understand the mechanism of oxidation inhibition. His CEMS results obtained by using Sn^{119} in $CaSnO_3$ source are shown in Fig. 4.2(a); while the CEMS results obtained by using the Fe^{57} in Rh source are given in Fig. 4.2(b). The spectrum corresponding to the as-implanted sample [Fig. 4.2(a)] shows the presence of an intermetallic compound $FeSn_2$ and a solid solution of FeSn at an average concentration of 4 at % of Sn. The spectrum corresponding to oxidation at 350°C reveals the formation of SnO_2 while the spectrum corresponding to the oxidation at 500°C shows the formation of another intermetallic viz. FeSn along with SnO_2. The Fe^{57} CEMS study [Fig. 4.2(b)] reveals that, upon oxidation at 350°C the unimplanted sample forms Fe_3O_4, while the implanted sample does not indicate any oxidation within the detection limit afforded by the CEMS technique. Also, subsequent to the oxidation at 500°C, 100% of the CEM spectrum of the unimplated sample is composed of Fe_2O_3 and Fe_3O_4 lines, while the spectrum of the implanted sample mainly shows α-Fe with less than 14% contribution of Fe_2O_3. These results clearly reveal a considerable inhibition of oxidation of iron upon tin implantation.

Dorik *et al.*[35] (Poona group) have recently studied the oxidation properties of iron implanted with nitrogen ions by using the CEMS technique. In these experiments 80 KeV N_2^+ ions were implanted on iron foils at a dose of 2×10^{16} ions/cm^2 and a number of such samples in the as-implanted form or subsequent to a vacuum annealing treatment were subjected to oxidation treatment in air at the temperature in the range between 300°C and 500°C for four minutes in each case. The CEMS as well as the conventional gravimetric measurements preformed on these samples

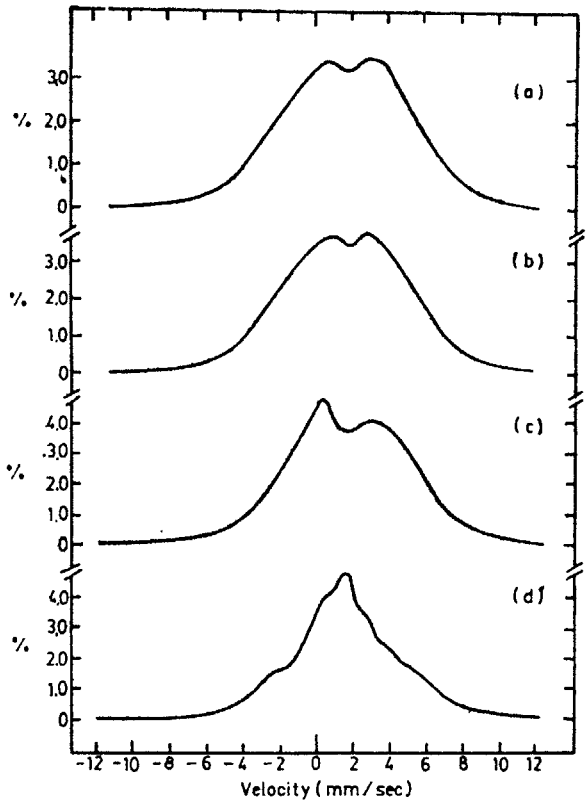

FIG. 4.2 (a) Room temperature Sn^{119} CEM spectra of iron implanted with Sn^{+} ions at a dose of 5×10^{16} ions/cm^2, oxidised at different temperatures for 20 minutes : (a') as implanted, (b') oxidised at 200°C, (c') oxidised at 350°C and (d') oxidised at 500°C.

revealed that the as-implanted samples exhibit an enhanced rate of oxidation as compared to the virgin iron foils. If one compares the spectra of Fig. 4.3 and 4.4(a) which correspond to the unimplanted and implanted samples oxidized at 300°C for 4 mins respectively, it is clear that the oxide components (Fe_2O_4 and Fe_2O_3) are dominant in the implanted case as compared to the case of the unimplanted sample. In fact, the ratio of the oxygen coordinated Fe to α-Fe has a value of 3.6 in the implanted case while a value of 0.96 in the case of the unimplanted sample. These differences in the oxidation rate were also confirmed by using gravimetric measurements. When the implanted foil which is annealed in a vacuum of 10^{-6} Torr at 300°C for 30 mins is oxidised, it shows a reduction in the oxidation rate even as compared to the rate exhibited by the virgin foil. This can be clearly seen by comparing the CEM spectra of Fig 4.3 and Fig. 4.5(a). The spectrum of Fig. 4.5(a) shows no detectable amount of the oxide fractions indicating thereby that the ion implanted and vacuum annealed foils show a significant improvement in the oxidation resistance of the virgin iron foils. This observation is once again in agreement

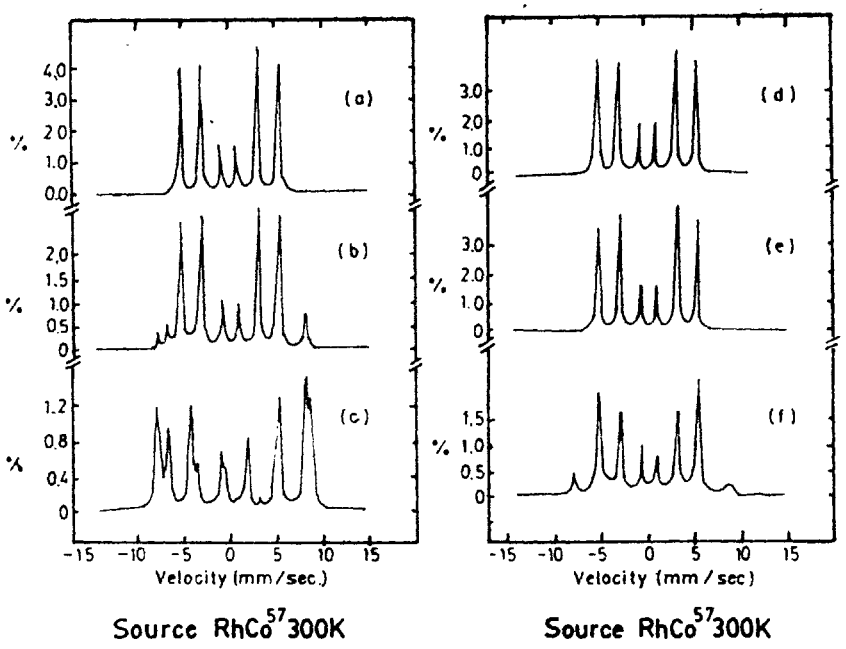

FIG. 4.2 (b) Room temperature Fe^{57} CEM spectra for unimplanted and implanted (5×10^{16} Sn^{+} ions/cm^2) iron, oxidised at different temperatures. Figures (a'), (b') and (c') correspond to the unimplanted iron foils oxidised at 200, 350 and 500°C respectively and (d'), (e') and (f') correspond to the implanted iron foils oxidised at 200, 350 and 500°C respectively.

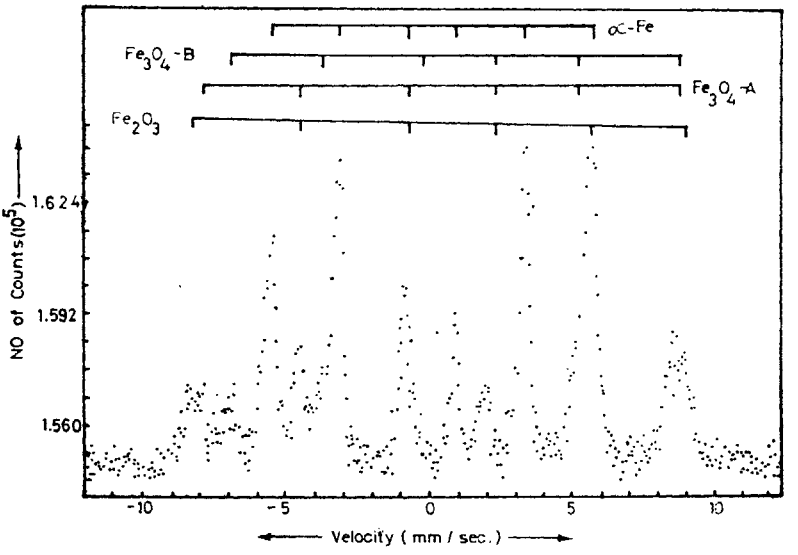

FIG. 4.3 Room temperature conversion electron Mössbauer spectrum of iron foil heated 300°C in air for 4 minutes.

of the gravimetric measurements. It may also be observed from Fig. 4.4 and 4.5 that at the oxidation temperature of 500°C both the implanted as well as the impalanted and annealed foils exhibit considerable oxidation.

It has been argued that ion implantation in iron produces defects and compressive stresses in the surface layers. Whereas the former effect enhances the oxidation rate due to defect assisted diffusion, the latter effect tends to inhibit it; the overall effect in the implanted sample being a reduction in oxidation resistance. The vacuum heat treatment (which is carried out at a temperature above the vacancy annealing temperature[44] for α-iron of 140°C but below its recovery temperature of 450°C) anneals out the point defects, stabilizes the compressive stresses and favours the magration of the implanted nitrogen atoms towards the grain boundaries and dislocation pipes leading to blockage of the short circuit paths for oxygen indifussion[18].

From the examples discussed in the above paragraphs it may be clear that the CEMS technique has a tremendous potential in investigating the properties of ion implanted metals and alloys which contain a suitable Mössbauer accessible

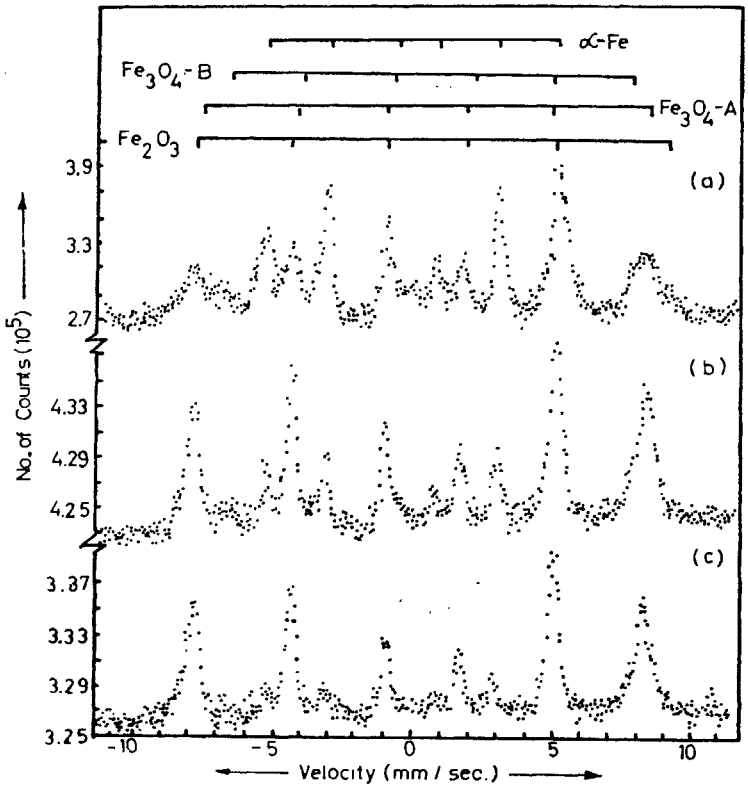

FIG. 4.4 Room temperature conversion electron Mössbauer spectra of N_2^+ implanted iron foil heated in air at (a) 300°C, (b) 400°C (c) 500°C for 4 minutes each.

element such as Fe or Sn. Very recently it has also been demonstrated that the CEMS technique is equally powerful in studying the physics of ion beam induced interface reactions, which have been a subject of considerable interest in recent years.

4.2. *Ion Beam Mixing : CEMS Studies*

The first experiments on the use of the CEMS technique for the studies of ion beam induced interface mixing and subsequent reactions were carried out very recently by the Poona University group [45–50]. The Ion beam induced interface reactions in the single interface Fe-Al (V. P. Godbole *et al.*)[45,47,50] Fe-Si (S. B. Ogale *et al.*)[44] and Fe-Ge (J. Patankar *et al.*)[44] structures have been investigated by this group, by using the Fe^{57} CEM Spectroscopy and interesting new information regarding the bombardment induced interface phenomena has been brought out. In all these studies, an iron film of a thickness of 300 Å was deposited onto the

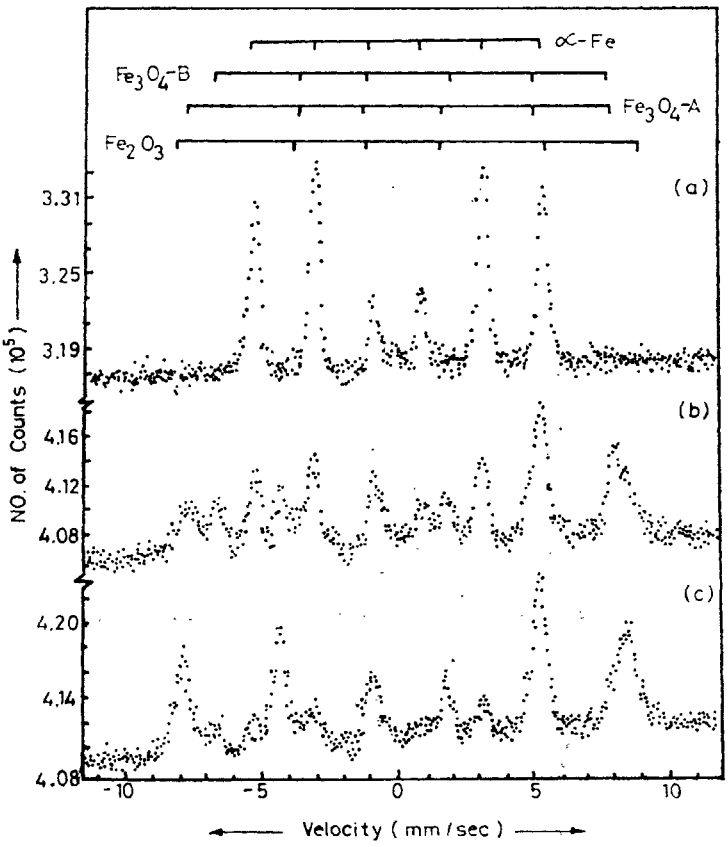

FIG. 4.5 Room temperature conversion electron Mössbauer spectra of N_2^+ implanted and vacuum annealed (300°C for 30 minutes) iron foils heated in air at (a) 300°C, (b) 400°C, (c) 500°C for 4 minutes each.

aluminium, silicon and germanium substrates conditioned by appropriate thermal and chemical treatments. Since ion beam mixing occurs at the interface and grows across it, a novel method of sample preparation was adopted to obtain the Mössbauer information predominantly from the interface region. For this purpose an ~ 50Å film of Fe^{57} Mössbauer isotope enriched to 95.45%was deposited on the substrates of Al, Si and Ge, followed by a deposition of an 250Å thick film of natural iron which contains only 2.2% of the Fe^{57} isotope (Fig. 4.6). Since the Mössbauer signal emanates only from the Fe^{57} nuclei, by using this sample preparation procedure an interface sensitive conversion electron Mössbauer spectroscopic study could be carried out and the early interface reactions in the ion beam mixed region could be revealed.

The first system in which the ion beam mixing process was characterised by the interface sensitive CEMS technique was Fe-Al. This system was chosen for the following reasons[47] : (i) Fe^{57}, a celebrated Mössbauer isotope is a constituent of one of the components of this system; (ii) the equilibrium solid solubility of Fe in Al is extremely low i.e. only 0.005 at. % even upto 450°C, with the result that the conventional thermal treatment does not lead to any substantial interface reaction in this system; which enables one to clearly identify the characteristic differences between the ion beam induced and pure thermal reactions at the interface of two elemental solids; (iii) the phase diagram of the Fe-Al system is extensively investigated and it shows the existence of a large number of phases such as Fe_4Al_{13}, FeAl, $FeAl_6$, Fe_2Al_5, Fe_3Al etc; which is a favourable situation in so far as the occurrence of mixing at the interface is concerned, as per the empirical rule established earlier; (iv) Al being a low-z material, it does not produce a high photoelectron background and thus the CEM spectra are expected to be of a good quality in the case of this system; and (v) Al being non magnetic, it does not create any complications in elucidating the magnetic hyperfine interactions at the Fe^{57} nuclei. Many Fe-Al samples,

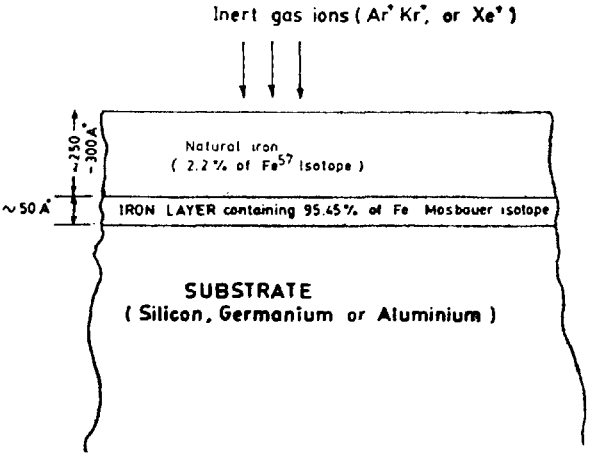

FIG. 4.6 Sample for the interface sensitive Conversion Electron Mössbauer Spectroscopic Studies.

prepared by following the procedure mentioned above, were implanted with 100 KeV Ar^+ ions at a dose range between 1×10^{16} to 3×10^{16} ions/cm^2 to achieve the interface mixing. The fact that the interface mixing has occurred was confirmed by Rutherford Backscattering measurements (Fig. 4.7), which also brought out the average composition of the mixed zone to be $Fe_{55}Al_{45}$. The as-deposited as well as ion beam mixed samples were annealed at a background vacuum of 10^{-6} Torr at various temperatures up to a maximum of 600°C and the transformations in the CEM spectra were monitored. All the spectra were computer analysed by following the conventionl Mössbauer fitting procedure along with the procedure for obtaining the distribution of magnetic hyperfine fields as outlined by window.

The CEM spectra of the as-deposited sample and the corresponding hyperfine field distribution are shown in [Fig. 4.8(a) and Fig. 4.8(e)] respectively. In addition to the h.f. field of 330 KOe corresponding to α-Fe, the h.f. distribution also shows another dominant magnetic interaction corresponding to a field value of ~240 KOe, and an intense low field component which could indeed be due to the quadrupole and not the magnetic interaction. The h.f. field of 240 KOe corresponds to the presence of three aluminium neighbours at the sites of a number of Fe^{57} nuclei near the interface region. This can happen due to the deposition induced reaction. The appearent low field magnetic component could indeed be fitted with a quadrupole doublet contribution having the h.f. interaction parameters of isomer shift $\delta = 0.33$ mm/s and quadrupole splitting $\Delta = 1.018$ mm/s. The appearance of this

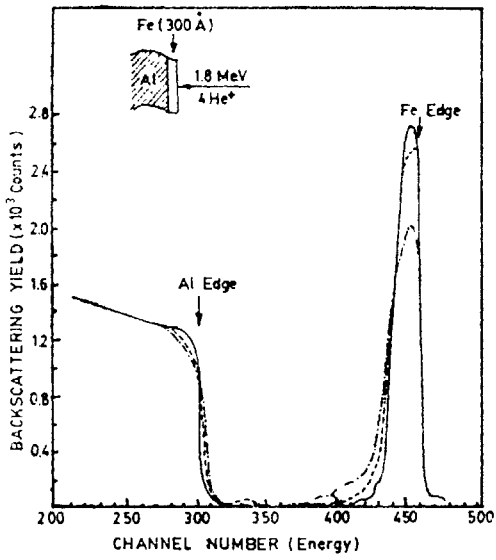

FIG. 4.7 Rutherford Backscattering Spectra (RBS) of the as-deposited and ion beam mixed composites. The————line corresponds to the as-deposited sample, the.....line corresponds to the sample bombarded with 100 KeV Ar^+ ions at a dose of 1×10^{16} ions/cm^2 and the-.-.-.-. line corresponds to the sample bombarded with 100 KeV Ar^+ ions at a dose of 3×10^{16} ions/cm^2.

doublet was attributed to the presence of Fe^{57} atoms in the γ-Al_2O_3 skin on the surface of aluminium[51] (This natural oxide of Al is always present on the surface of aluminium in the form of an ultra-thin film). When bombarded with Ar^+ ions the CEM spectrum shows a drastic change [see Fig. 4.8(b) and Fig. 4.8(f) for the field distribution [P(H) curve]. Figure 4.8(f) shows a considerable reduction of the peak at 330 KOe corresponding to α-Fe and emergence of low field components at field values of 100 KOe, 190 KOe and 252 KOe. It may be hypothesized that the local atomic coordination in the ion beam mixed region fluctuated randomly between the aluminium like (i.e. f.c.c.) and iron-like (i.e. b.c.c.) environments. The peaks at 192 koe and 252 kOe can thus be attributed to the fluctuations of atomic coordination between 8 to 12 neighbour environments. The peak at 100 KOe (lower field) can possibly be attributed to the dilute magnetic alloy of Fe in aluminium on the aluminium side of the interface.

When the ion beam mixed sample is annealed at 300°C and 400°C for twenty minutes in each case, the corresponding CEM spectra [Figs. 4.8(c) and 4.8(d)] and the field distributions [4.8 (g) and 4.8(h)] do not show any significant changes from the characteristics exhibited by the ion beam mixed sample. When annealed at

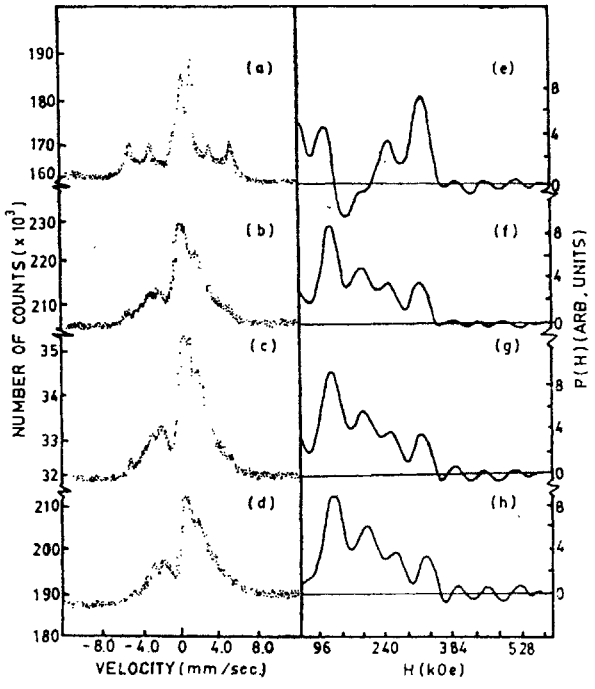

FIG. 4.8 Room temperature Conversion Electron Mössbauer Spectra of (a) as-deposited and (b) ion beam mixed Fe-Al composite. The spectra (c) and (d) represent ion beam mixed samples annealed at 300°C and 400°C respectively for 20 minutes each. The curves in figs. (e), (f), (g) and (h) are the hyperfine field distribution plots corresponding to the spectra in (a), (b), (c) and (d) respectively.

500°C for twenty minutes, however, the spectral features show a drastic change, and the standard computer fitting procedure reveals the presence of α-Fe and Fe_3Al phases[53] in the sample (Fig. 4.9). This sample when further annealed at 600°C, shows another drastic change in the CEM spectrum, which now indicates the presence of a small contribution of α-Fe and a large contribution of a central doublet component. The h.f. interaction parameters corresponding to the doublet match reasonably well with the parameters corresponding to the iron clusters in aluminium matrix[52].

When the as-deposited sample was annealed at various temperatures upto 500°C. the spectra continued to show the presence of α-Fe with an increase in the intensity of this spectral component and a gradual reduction of the central doublet corresponding to Fe^{57} in Al_2O_3 skin, which could be due to the out-diffusion of iron from the oxide. No Fe_3Al phase was observed in the case of the as-deposited sample annealed at 500°C, which showed the presence of only α-Fe. This clearly brings out the difference between the characteristics of the thermally induced interface reactions in the as-deposited and ion beam mixed samples.

The Poona group has also studied the dose dependence of ion beam mixing at the Fe-Al interface[57]. For this purpose, non-interface sensitive studies were carried out; in which the samples were prepared by depositing iron overlayer, containing~

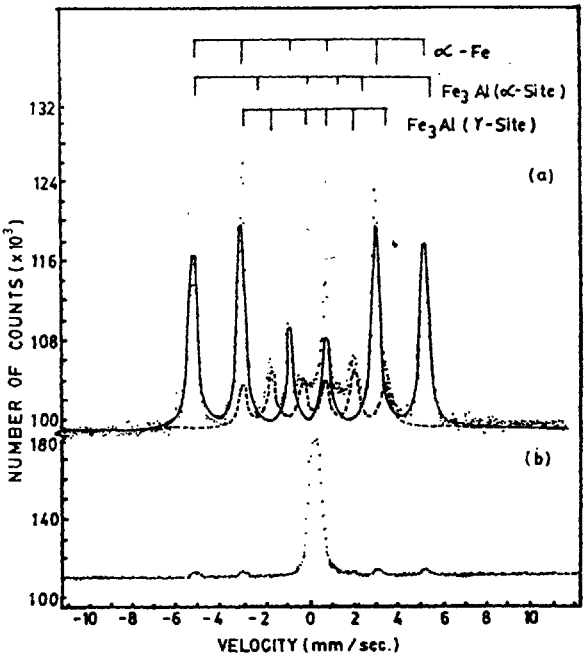

FIG. 4.9 Room temperature Conversion Electron Mössbauer Spectra of ion beam mixed samples annealed (a) at 500°C showing the precipitation of Fe and Fe_3Al phases, and (b) at 600°C showing the formation of iron clusters.

30% of the enriched Fe^{57} isotope uniformly distributed over the film region onto the aluminium substrates. Such non-interface sensitive studies were undertaken primarily to understand the nature of the change in the beam mixing process when the ion dose is raised from a low value of less than $\sim 5 \times 10^{14}$ ions/cm^2 at which individual cascade effects dominate, to the high doses at which the cascade overlap effects start playing an important role. The non-interface sensitive method was used in the place of the interface sensitive one in these studies because the interface sensitive technique defines a fixed length scale (of $\sim$ 50 Å) at the interface, which is not compatible to the growth of the mixed region as a function of the increase of the ion dose. The results of the non-interface sensitive CEMS studies are shown in Fig. 4.10.

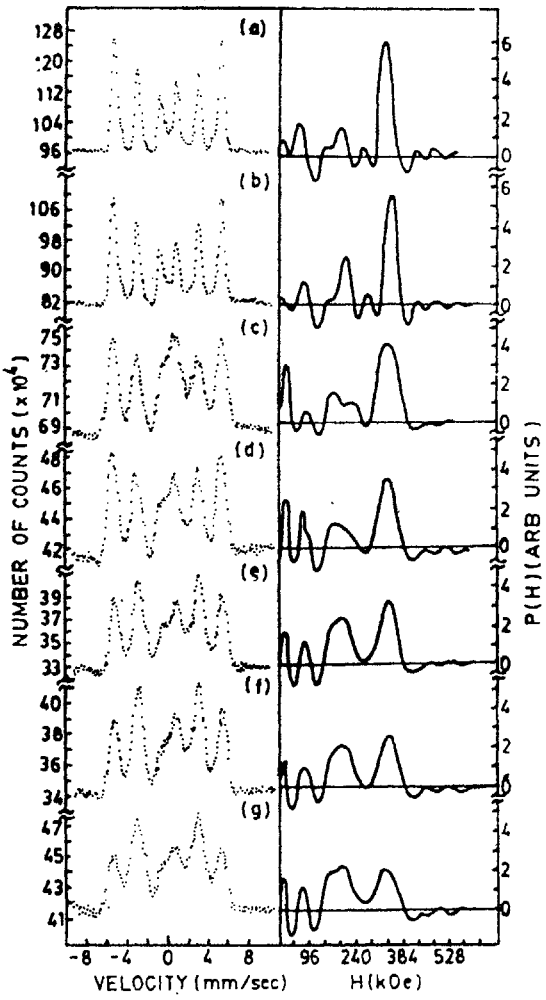

FIG. 4.10 Room temperature CEM spectra of (a) as deposited Fe-Al composite and ion beam mixed Fe-Al composite with a dose of (b) 1×10^{14} ions/cm^2, (c) 5×10^{14} ions/cm^2 (d) 1×10^{15} ions/cm^2, (e) 5×10^{15} ions/cm^2, (f) 1×10^{16} ions/cm^2, (g) 3×10^{16} ions/cm^2. The corresponding hyperfine field distribution curves are represented with continuous curves.

In Figure 4.10(a) the CEM spectrum of the as-deposited sample is shown while in Fig. 4.10(b) to 4.10(g) the CEM spectra of the composites implanted with Ar^+ ions at various values of ion dose ranging between 10^{14} ions/cm^2 to 3×10^{16} ions/cm^2 are shown. The distributions of internal magnetic field have also been given for all the specta. The distribution corresponding to the as-deposited sample exhibits a peak at 330 KOe (which corresponds to α-Fe) and other small variations which can partly be attributed to the use of Fourier series in the decomposition procedure upon ion beam mixing. With increasing implantation dose the peak at 330 KOe shows a systematic decrease in intensity with emergence of peaks corresponding to lower values of hyperfine fields. Also the line widths of the Mössbauer spectral components show an increase with implantation dose, indicating the presence of disorder in the mixed zone. The emergence of peaks corresponding to lower field values is due to formation of an interface alloy in which the Fe^{57} nuclei find one or more of aluminium neighbours which contribute to the decrease of hyperfine field. When integrated over the entire range of lower field values distinguishable from the peak at 330 KOe, the total low field contribution shows an almost exponential rise with ion dose (Fig. 4.11). It may be noted however, that the rise is almost linear upto a dose of 10^{15} ions/cm^2 beyond which the nature of the curve and hence possibly the mixing process, shows a derivation[9]. It is interesting to note that the dose value of 10^{15} ions/cm^2 is typically the value at which the cascade overlap effects may be expected to dominate the mixing process.

Another binary system on which the ion mixing work has been carried out by the Poona group by employing the CEMS technique is Fe-Si (S. B. Ogale *et al.*)[48]. Apart from the fact that this system offers many advantages similar to those mentioned in the case of the Fe-Al system, the Fe-Si system can serve as a representative

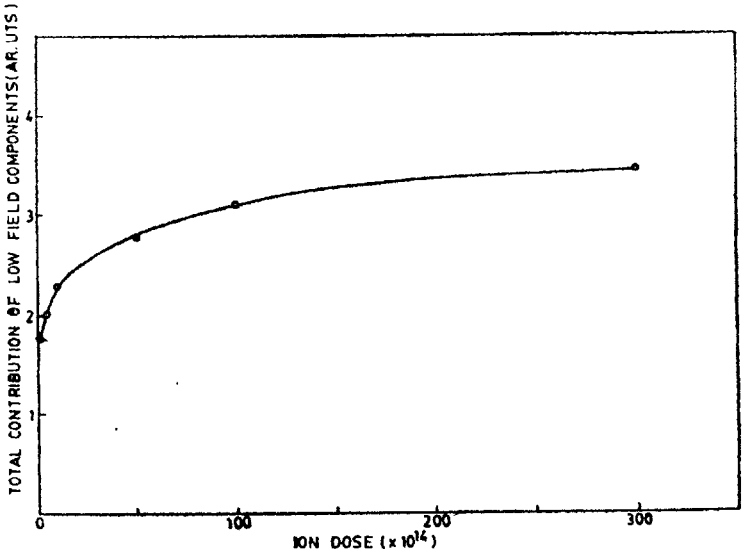

FIG. 4.11 Total contribution of low field component as a function of ion dose for Fe-Al composite.

of the 3d-transition metal silicides which are extremely useful in applications. The CEM spectra of the as deposited and ion beam mixed samples and the corresponding field distributions are shown in Fig. 4.12(a,b). It can once again be seen that ion beam mixing leads to an enhancement in the intensity of the low field components due to the incorporation of nonmagnetic silicon atoms in the iron matrix. Upon annealing at various temperatures upto a maximum of 700°C the ion beam mixed sample passes through various stages of recovery (see Fig. 4.13) leading finally to the precipitation of Fe_3Si phase. The as deposited sample on the other hand shows a diffusion limited interface reaction leading to the formation of only avery small quantity of Fe_3Si. In order to further reveal the interesting features of the interface reactions, we carried out resistance annealing measurements on the as-deposited as well as ion beam mixed samples. The results of these measurements (Fig. 4.14) are found to be in agreement with the results of CEMS measurements.

In addition to the Fe-Al and Fe-Si systems, the ion beam induced interface reactions have also been studied in the case of the Fe-Ge system by employing the CEMS technique. In these experiments the germanium substrates were prepared on

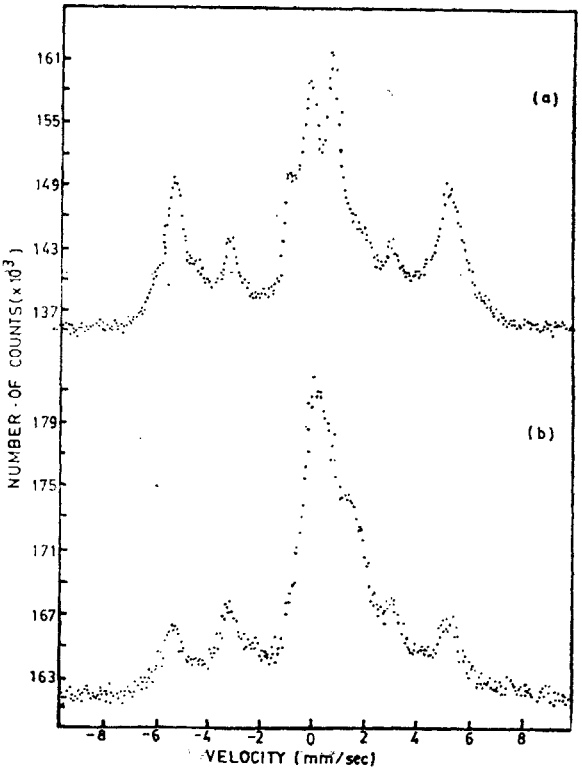

FIG. 4.12 (a) Room temperature Conversion Electron Mössbauer (CEM) spectra of (a') as-deposited and, (b') ion beam mixed (IBM) Fe-Si composites.

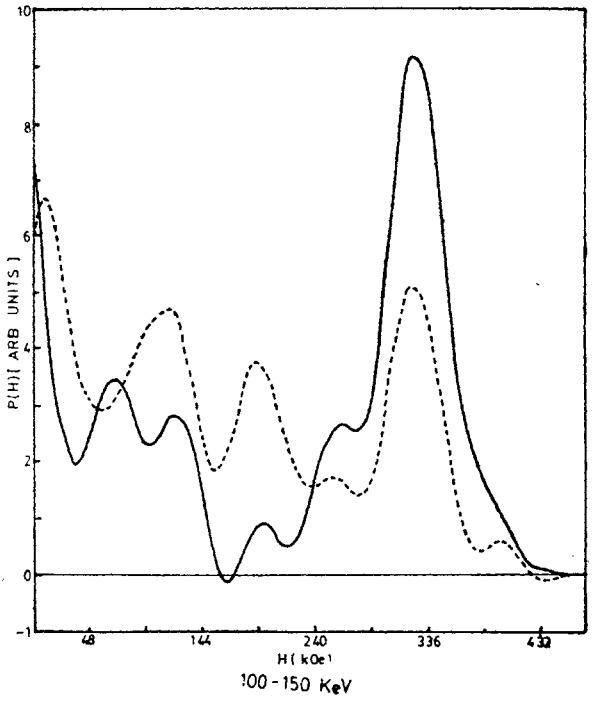

4.12 (b) The hyperfine field distribution P(H) curves for the as-deposited (solid line) and ion beam mixed (dashed line) Fe-Si composites.

the SiO_2 layers thermally grown on single crystal silicon surface; by vacuum evaporation method. Such substrates were then deposited with an ~ 50Å thick layer of Fe^{57} isotope enriched to 95.45% and subsequently with a 250A° thick layer of natural iron, as in the case of the interface sensitive studies on Fe-Al and Fe-Si systems. The CEM spectra corresponding to the as-deposited and ion beam mixed samples in the as-prepared form and subsequent to thermal annealing treatments at various temperatures upto a maximum of 625°C are shown in Fig. 4.15. These results once again clearly bring out the differences between the ion beam induced and purely thermal interface reactions. For detailed discussion regarding these spectra the reader is referred to the publication.

In the earlier paragraphs we discussed the work of basic nature concerning the ion beam mixing process which has been carried out by employing the CEMS technique. Using the same techniques the Poona group has also carried out an investigation of applied nature on the ion beam mixed state of Fe-Al alloy, in which the electro-chemical corrosive properties of this alloyhave been studied[47]. In these experiments the as-deposited as well as ion beam mixed Fe-Al samples prepared for interface sensitive CEMS measurements were subjected to electro-chemical corrosion by employing the three-sweep potentio-kinetic polarization technique at a sweep rate of 10 mv/s.

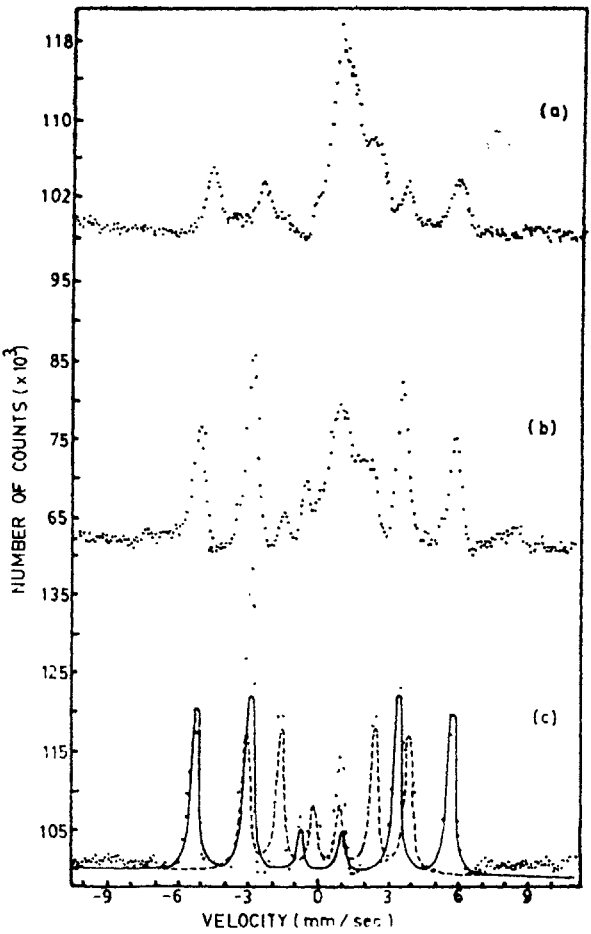

FIG. 4.13 Room temperature Conversion Electron Mössbauer Spectra of ion beam mixed Fe-Si composite vacuum annealed at (a) 240°C, (b) 450°C, (c) 700°C for one hour in each case. Subspectrum shown with dashed line in Fig. (c) shows the sextet corresponding to the Fe_{II} site! of the Fe_3Si phase while the other subspectrum (solid line) shows the sextet corresponding to α-Fe with an overlap of the contribution of site of Fe_3Si.

From Fig. 4.16(a), it is observed that the Fe foil clearly shows active to passive transition. In the case of aluminium, no active to passive transition is observed [Fig. 4.16(b)] because, subsequent to an initial dissolution, the passivation ensues almost immediately due to the formation of an aluminium oxide coating in the aqueous medium.

When the as-deposited sample was subjected to electrochemical corrosion, the iron layers deposited on the aluminium substrates dissolved completely [Fig. 4.17(a)]. On the other hand, the ion beam mixed Fe-Al sample exhibited distinctly different features as compared to as-deposited Fe-Al sample [Fig. 4.17(b)]. An examination of [Fig. 4.17(a) and Fig. 4.17(b)] clearly shows that the dissolution of iron is

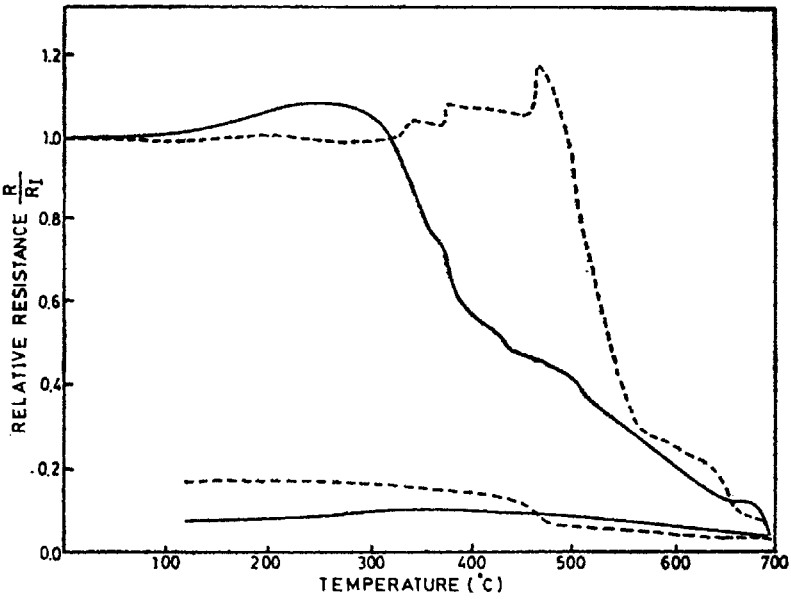

FIG. 4.14 Resistance-annealing curve for the as-deposited (solid line) and ion beam mixed (dashed line) Fe-Si composites.

considerably higher in the as-deposited sample as compared to the ion beam mixed the curve sample. This is indicated by the current density corresponding to the point G on of the first negative going sweep. It is also observed that the as-deposited sample does not show any active-passive transition and indicates a dissolution similar to that of pure aluminium.

In order to reveal the physics of the corrosive properties exhibited by the ion beam mixed sample we characterised this sample before and after the corrosive action by using the CEMS technique. The CEM spectrum of the ion beam mixed sample [Fig. 4.18(b)] is significantly different as compared to that of the as-deposited sample [Fig. 4.18(a)] and the corresponding magnetic field distribution [Fig. 4.18(e)] shows four peaks at 100 KOe, 192 KOe, 252 KOe and 330 KOe. On comparing [Fig. 4.18(d)] with [Fig. 4.18(e)], it is clearly seen that the peak at 330 koe which corresponds to α-Fe is considerably reduced and low field components are increased upon ion bombardment. This means that significant atomic mixing has occurred at the interface. The average composition of the mixed layers obtained by RBS technique turns out to be $Fe_{55}Al_{45}$. The details of this CEM spectrum and the corresponding field distribution have already been discussed earlier in this report. In the present context it may only be mentioned that the ion beam mixed interface is a disordered alloy with significant fluctuations in local alloy structure and composition.

When subjected to corrosion the ion beam mixed sample leads to CEM spectrum as shown in Fig. 4.18(c). When decomposed, this spectrum gives magnetichy perfine

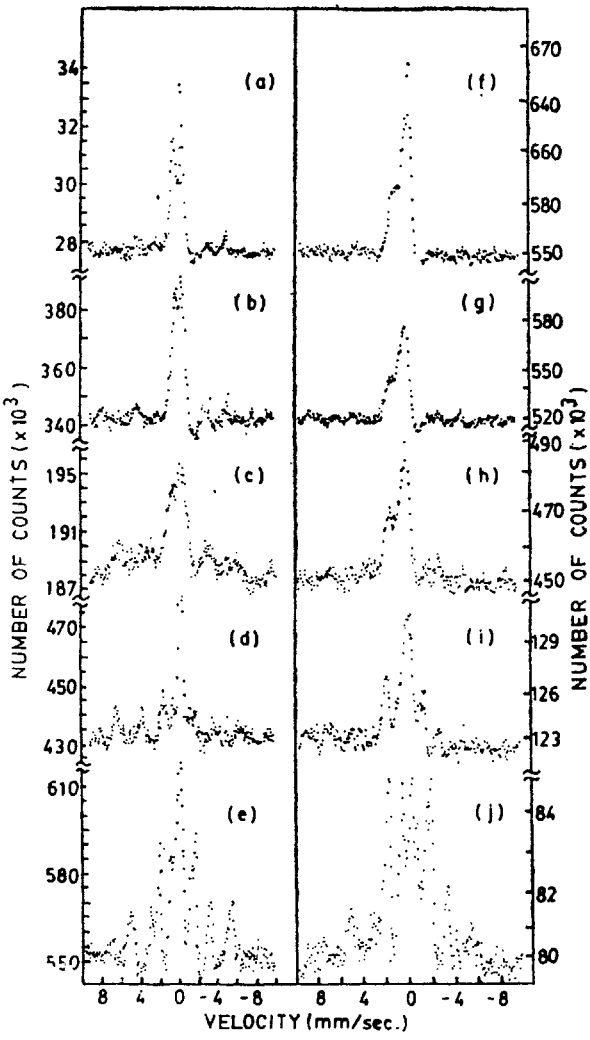

FIG. 4.15 Conversion Electron Mössbauer (CEM) spectra of (a) as-deposited and (f) ion beam mixed Fe-Ge composites. CEM spectra in figures b(g), c(h), d(i) and e(j) correspond to the as-deposited (ion beam mixed) sample annealed at 200°C), 350°C, 500°C and 625°C respectively, for one hour each.

field distribution as given in Fig. 4.18(f). It can be readily seen that the peaks at 192 KOe and 252 KOe, in the field distribution corresponding to the ion beam mixed sample are decreased substantially upon corrosion while the peak at ~ 100 KOe is shifted to a lower field value of ~ 90 KOe. It is also observed that the peak at 330 koe is decreased to a certain extent. In addition to these changes in the magnetic components we could fit the total spectrum of Fig. 4.18(c) with two quadrupole-split doublets. One of the doublets has an isomer shift of 0.40 mm/sec and a quadrupole splitting of 0.63 mm/sec, while other doublet has an isomer shift of 0.89 mm/

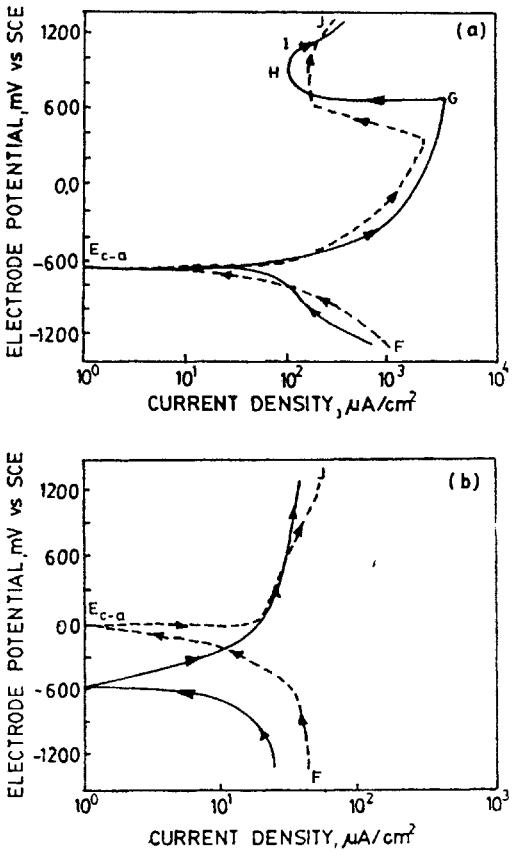

FIG. 4.16 Second positive going sweeps in the three sweep potentio-kinetic polarization curves for (a) pure iron foil and (b) pure aluminium foil. The full line (———) and dashed (- - -) curves correspond to sweep rates of 1.33 mV/sec and 10 mV/sec respectively.

sec and a quadrupole splitting of 1.27 mm/sec. The hyperfine parameters of the latter doublet match resonably well with those of FeO[54–56] (I. S. = 0.91 mm/sec.; Q. S. = 0.80 mm/sec) except for a higher value of the quadrupole splitting which may be attributed to the thinness of the ion beam mixed film and to the damage imparted to the interface structure due to the ion bombardment. The hyperfine parameters of the other doublet can be favourably compared to those of hydrated nonmagnetic oxides of Fe[53–56] such as, γ-FeOOH (I. S. = 0.38 mm/sec. Q. S. = 0.59 mm/sec), β-FeOOH, (I. S. = 0.37 mm/sec., Q. S. = 0.71 mm/sec. and also α-Fe_2O_3 clusters[57] (I.S. = 0.31 mm/sec. and Q. S. = 0.98 mm/s). As indicated earlier, the local atomic coordinations in the ion beam mixed alloy fluctuate within the mixed region and hence formation of two or more phases of the above type is indeed possible.

4.3. *Laser Treatment : CEMS Studies*

As mentioned earlier the laser treatment has emerged as a powerful material processing technique in recent years. Applications of CEMS technique to the study of the physics of laser-solid interactions have begun to appear in literature only very recently and in what follows, as have discussed a few such cases to serve as illustrations.

Petrikin *et al.*[58] carried out very interesting experiments by using laser irradiation as an alternative to diffusion and ion implantation, to incorporate iron dopants from a deposited layer into the bulk of silicon. A typical spectrum of a sample with an iron layer (30 μg/cm^2) deposited on silicon and irradiated with 2.6 J/cm^2 is shown

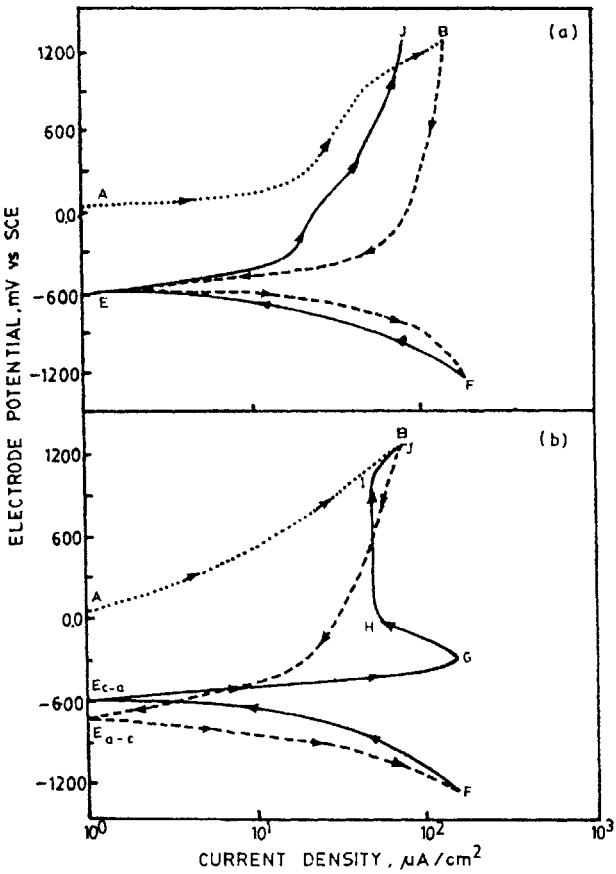

FIG. 4.17 Three sweep potentio-kinetic polarization curves for (a) as-deposited and (b) ion beam mixed, Fe-Al composite. The dotted (.....) curve corresponds to 1st positive going sweep, the dashed (- - - -) curve corresponds to 1st negative going sweep and the full line (————) curve corresponds to 2nd positive going sweep at the sweep rate of 10 mV/sec.

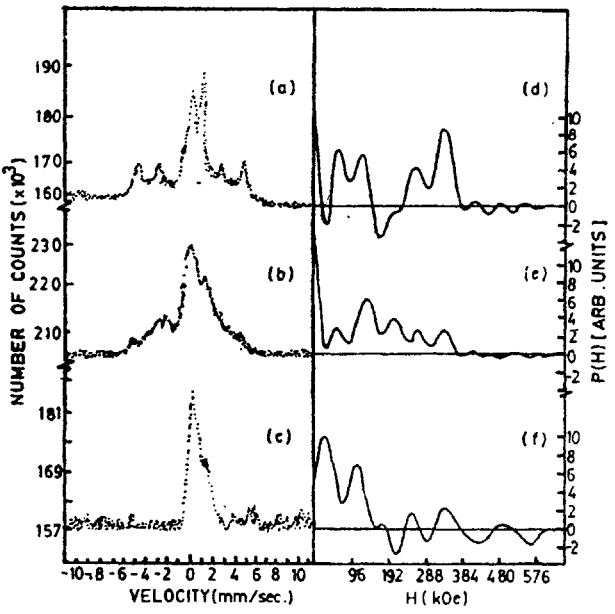

FIG. 4.18 Room temperature conversion electron Mössbauer spectra of Fe-Al composite : (a) as-deposited (b) ion beam mixed and (c) ion beam mixed composite subjected to aqueous corrosion. Hyperfine field distributions corresponding to the spectra in (a), (b) and (c) are shown in (d), (e) and (f) respectively.

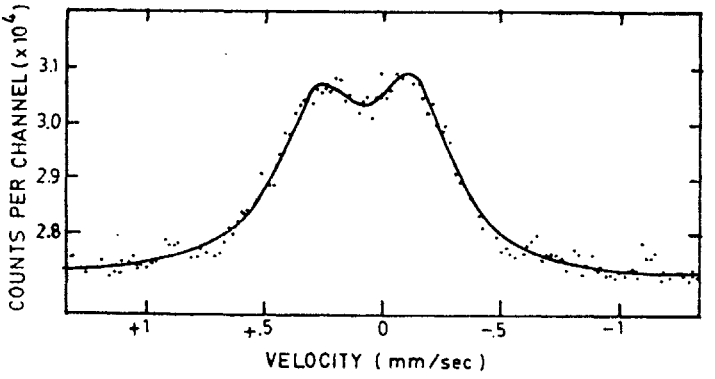

FIG. 4.19 Room temperature CEM spectrum of a sample (Fe^- implanted in Si) irradiated with 2.6 J/cm² laser pulse.

in Fig. 4.19. The Mössbauer lines in the spectra are interpreted as components of a quadrupole-split doublet (I.S. = 0.2 mm/sec relative to α-Fe and Q. S. = 0.40 mm/sec) due to $FeSi_2$[59]. The nature of this spectrum did not exhibit any change upon the stripping up of surface layers upto a depth of 3500Å, except for a decrease in intensity. This laser induced diffusion of iron atoms can be explained on the basis of the liquid phase model. It was also observed that with the use of a low power

density (1—0.6 J/cm²) of laser irradiation, iron atoms could not be incorporated below 100Å from the surface. Though the concentration of iron atoms diffused inside silicon was very high, the penetration was observed to be only in shallow surface layers. This can be due to the solid phase nature of the interface reaction induced by the laser irradiation at a low power density.

Experiments of the type discussed above have also been reported by Prasad[60]. In this investigations, an iron film (100Å) of enriched Fe^{57} isotope was deposited on polycrystalline Al foil and such samples were irradiated with a pulsed ruby laser ($\lambda = 0.693\ \mu m$) having a pulse width of 25 ns and an energy density in the range of 0–4 J/cm². Figure 4.20 shows CEM spectrum of the Fe-Al sample irradiated with a single 3.6 J/cm² laser pulse, alongwith the CEM spectra of the laser treated samples which were thermally annealed at 300°C, 500°C, 600°C and 630°C for 20 minutes

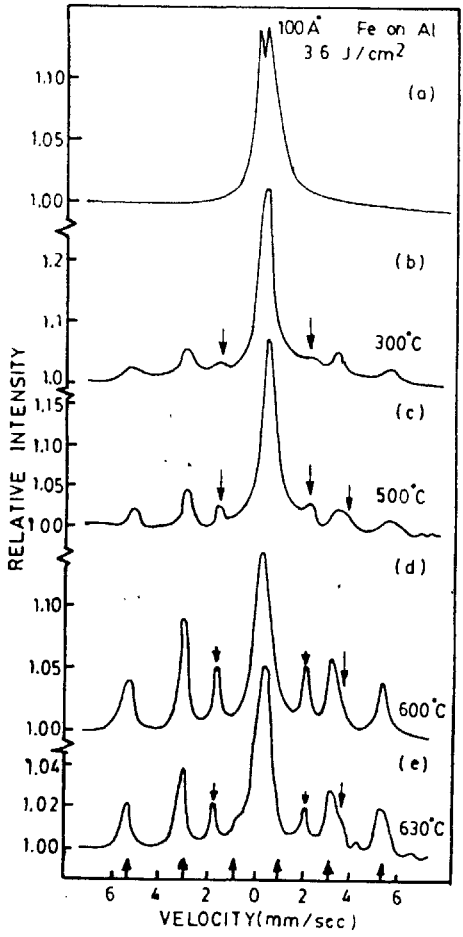

FIG. 4.20 Room temperature CEM spectra of Fe-Al composite irradiated with 3.6 J/cm² laser pulse (top) and subsequent thermal annealing.

in each case. The spectrum of Fig. 4.20(b) shows the presence of a quadrupole doublet (I.S. = 0.19 mm/sec, Q. S. = 0.4 mm/sec) and a singlet (I.S. = 0.43 mm/sec) having a small intensity. These Mössbauer parameters correspond to Fe dimers and monomers in Fe-Al system[52]. The CEM spectra of the vacuum annealed samples show development of resonance lines characteristic of α-Fe, Fe rich clusters, Fe_3Al and $Al_{12}Fe_4$[52]. This brings out the nonequilibrium nature of the pulsed laser irradiation process. The spectra shown in the work of Prasad also bring out that laser induced amorphasization is quite insignificant in the case of nanosecond pulsed laser treatment.

Recently, Dektiyar *et al.*[61] have reported CEMS studies on Laser irradiated Nb-Fe binary systems. They have basically investigated the redistribution of elements and formation of intermetallic compounds near the Nb-Fe boundary subsequent to laser irradiation. The CEM spectrum of a sample having niobium layer deposited on Fe^{57} layer shows no resonant absorption due to the attenuation of conversion electrons in the niobium over layer. When irradiated with the laser beam ($\lambda = 1.06\ \mu m$) the sample yields a CEM spectrum which shows the presence of distorted α-Fe lines [Fig. 4.21(a)] and this observation can be explained on the basis of the directed diffusion of iron atoms across the Nb-Fe interface which is connected with the directed defect generation by the laser action. Dektiyar *et al.*[61] also observed that the change in the sequence of layer deposition i.e. deposition of Fe^{57} on Niobium results in completely different laser induced reactions (Fig. 4.21(b)). In this case, the spectrum of the as-deposited sample shows a six finger pattern corresponding to α-Fe; however, upon laser irradiation the magnetic spectrum is found to transform into a quadrupole doublet (I.S. = 0.05 mm/sec. Q. S. = 0.28 mm/sec) which can be attributed to the formation of the $NbFe_2$ Phase[61]. These studies once again bring out the potentialities of the CEMS technique in the studies on laser treated materials.

5. Applications of Conversion Electron Mössbauer Spectroscopic (CEMS) Technique in Other Fields

In view of its simplicity and potentiality in bringing out the Mössbauer information regarding the submicron layers on solid surfaces the CEMS technique has found

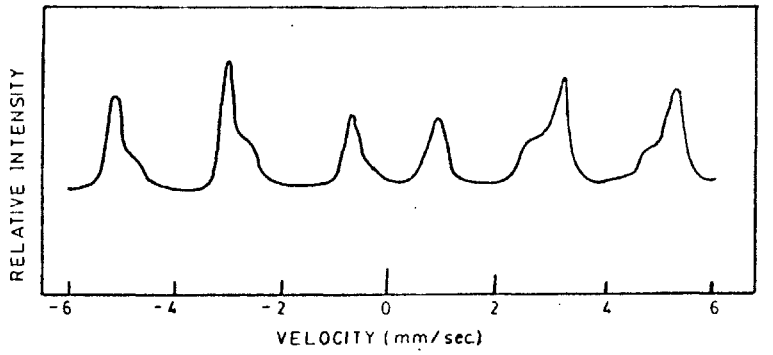

FIG. 4.21 (a) Room temperature CEM spectrum of Laser treated Nb-Fe couple.

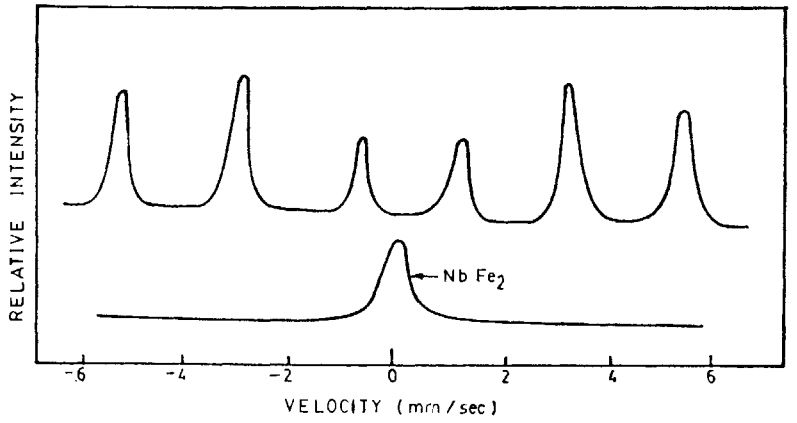

FIG 4.21 (b) Room temperature CEM spectra of Laser treated Fe-Nb composite.

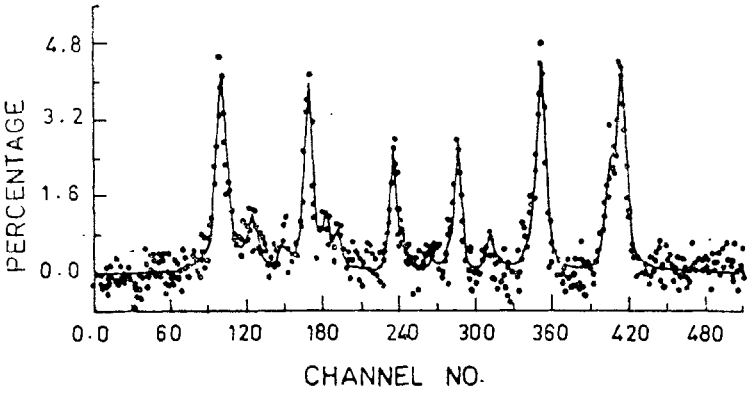

FIG. 5.1 (a) Room temperature CEM spectrum of steel sample corroded at 310°C for 1 day (10.5 pH, oxygen low).

numerous applications in other fields of Material Science. These applications include diversified areas such as oxidation and corrosion phenomena, magnetism in thin films, thermal reactions near surfaces and interfaces, structural and magnetic relaxations near the surfaces of amorphous metallic alloys etc. In the following paragraphs, we have briefly discussed some such applications, meant only to serve as illustrations and not to indicate the entire scope of the subject.

Jaggi *et al.*[14] have used the CEMS technique to study the high temperature corrosion of plain carbon steels in alkaline water which is an important investigation in the context of nuclear pressurized water reactors (PWR). Two typical spectra obtained by these authors for steel samples corroded in a solution of 10.5 *p*H at 310°C but corresponding to one and seven days of corrosion time, have been reproduced in Fig. 5.1(a) and Fig. 5.1(b) respectively. The differences in the spectral features clearly bring out the sensitivity of CEMS technique to the corrosive reactions

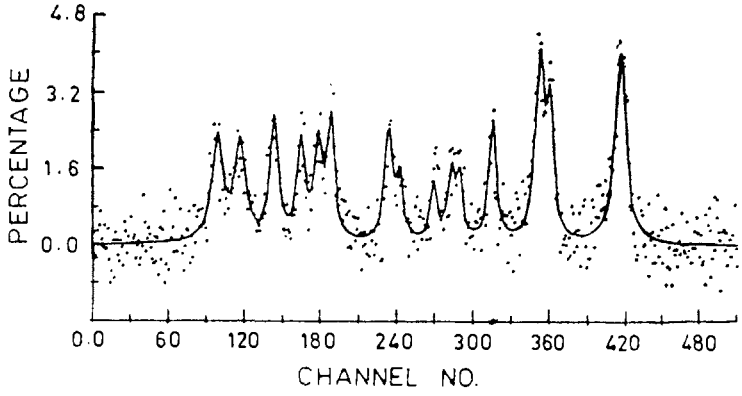

FIG. 5.1 (b) Room temperature CEM spectrum of steel sample corroded at 310°C for 7 days (10.5 pH, oxygen high).

occurring near surfaces. Through a series of systematic studies of corrosion products formed under differing conditions of the ambient, these authors have brought out the formation of non-stoichiometric $Fe_{3-\nu}O_4$ oxide in the initial phase, its growth at the oxide-electrolyte interface, as well as the approach of its composition to Fe_3O_4. With the increase in the oxygen content of the ambient to a value of .3 ppm the corrosion has been shown to be inhomogeneous, with the formation of an initial film which contains both α-Fe_2O_3 and spinel $Fe_{3-\nu}O_4$.

Another interesting application of CEMS technique in the studies of oxidation is the Mössbauer depth profiling method demonstrated by Bayreuther[36]. This method uses a special sample preparation technique which employs the use of a thin probe layer of enriched Fe^{57} isotope at a given depth below the iron surface. By changing the depth of the position of this probe layer below the surface, it has been shown that a resolution of $\sim$ 5Å can be obtained in ascertaining the location of the oxide-metal interface. This method is especially useful in the context of early oxidation studies, since it can yield an information regarding composition, stoichiometry and chemical nature of oxide films having thickness of less than $\sim$ 100Å.

Metallic glasses have emerged as scientifically interesting and technologically important materials in recent years. Since many of these materials involve iron as a component, Mössbauer spectroscopic techniques have found a central role in the studies on these systems. A considerable work on the bulk properties of metglasses has already been carried out by using the Mössbauer transmission technique, and work employing the scattering Mössbauer techniques has just begun to appear. Nasu and Gonser[62] have reported results of simultaneous transmission and scattering measurements on $Fe_{40}Ni_{40}P_{14}B_6$ metallic glass. It has been shown by these authors that the surface atoms have 10% higher average hyperfine field as compared to the bulk atoms; the line-width obtained in the case of the scattering Mössbauer spectrum are larger than those in the transmission spectrum and the intensities of 2nd and 5th lines in the surface spectrum are 27% larger in area as compared to the

case of the bulk spectrum. Ok and Morrish[63] have reported on observation of magnetic an isotropy in the surface and bulk regions of a thermally annealed $Fe_{82}B_{12}Si_6$ metglass sample by carrying out CEMS and transmission measurements. These authors have shown that the surface region recrystallizes at a temperature lower than the glass transition temperature (T_g) leading to generation of stresses and hence anisotropy of magnetization. The fact that the dull surface of the metglass crystallizes faster than the shiny surface at a given temperature below T_g has also been demonstrated in these studies. Recently, we (Poona group) have performed systematic studies of structural relaxation and diffusive transport near the surface of $Fe_{67}Co_{18}Si_1B_{14}$ metglass by employing the CEMS technique[64]. It has been shown that annealing of this metglass in vacuum at 300°C for 10 hrs. does not show significant changes in the hyperfine field distributions; however, annealing at 390°C (i.e. 40°C below $T_g = 430$°C) leads to atomic transformation leading to Fe_3B-like atomic order. On annealing at 440°C (i.e. above T_g) for ten hours, three phases viz. Iron with substitutionally dissolved cobalt[65]. Fe_2B[66] and Fe_5SiB_2[66] are seen to precipitate (see Fig. 5.2). We have also carried out CEMS studies on the thermally induced transformations in the samples of the same metglass coated with a 300Å over layer of iron enriched to 33% with Fe^{57} atoms. It has been shown that a deposition induced reaction leads to the formation of an interface phase close in

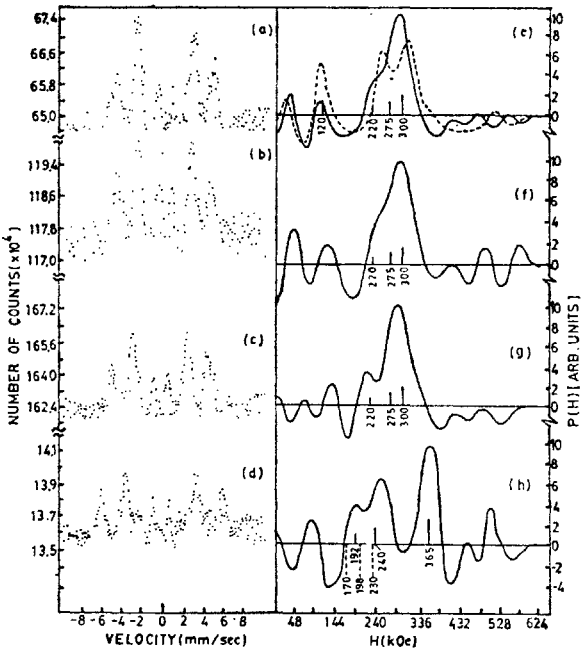

FIG. 5.2 Conversion electron Mössbauer spectra of the front (Shiny) surface of the as-received metglass (a), and metglass annealed at 300°C (b), 390°C (c), and 440°C (d), for ten hours each. The hyperfine field distributins [P(H)] curves corresponding to the CEM spectra in (a), (b), (c) and (d) are shown in (e), (f), (g) and (h) respectively. The dashed line in (e) shows the P(H) curve corresponding to the CEM spectrum of the back (dull) surface.

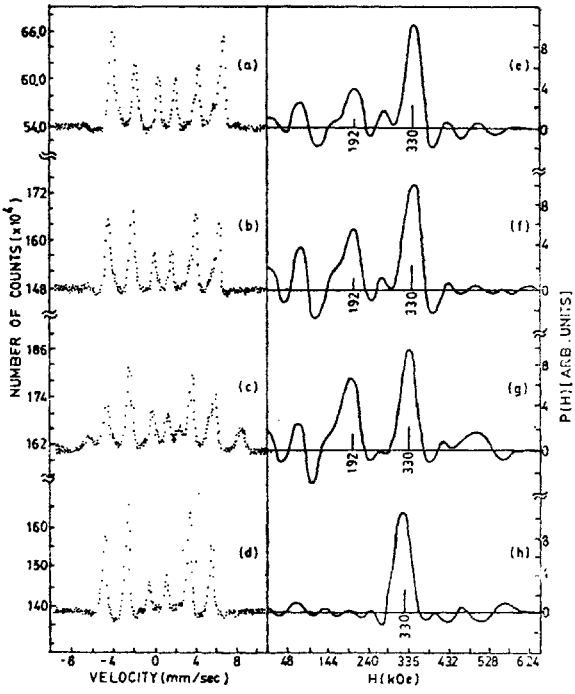

FIG. 5.3 Conversion electron Mössbauer spectra of the metglass deposited with 3 00Å iron overlayer in the as-deposited form (a); and subsequent to annealing of the composite at 300°C (b) 390°C; (c) and 440°C; (d) for ten hours each. The hyperfine field distribution (P(H) curves) corresponding to the CEM spectra in (a), (b), (c) and (d) are shown in (e), (f), (g) and (h) respectively.

composition to Fe_5SiB_2 (peak at h.f. field of 192 koe, see Fig. 5.3) and it grows upon thermal annealing at 300°C and 390°C for ten hours. This has been attributed to the (out) diffusion of Si and B (metalloid) atoms and the corresponding diffusion coefficients have been estimated to have values of 6.3×10^{-19} cm^2/sec. and 1.4×10^{-18} cm^2/sec. at 300°C and 390°C respectively. These are indeed in the range of values expected in the case of glassy metals[67]. The differences in the surface (back and front) and bulk atomic arrangements even in the as-quenched glass and their thermal transformation behaviour have also been brought out in these studies for the first time. Figures 5.2 and 5.4 demonstrate the differences in the field distributions near the shiny (front) surface, dull (back) surface and the bulk region in the case of the as-quenched glass. Comparison Fig. 5.2 and 5.4 also brings out the differences in the thermally induced transformations near the shiny surface and the bulk.

From the examples discussed in this subsection it is clear that the technique of Conversion Electron Mössbauer Spectroscopy (CEMS) has a major role to play in the field of material science, especially in the context of submicron physics.

Conclusions

In view of the important role played by surfaces and interfaces in a variety of physical and chemical processess, there is a growing interest in both the modification of surfaces to the required specifications and characterization of surfaces at the atomic level. Recently developed techniques of directed energy processing of surfaces such as ion implantation, ion beam mixing, electron and laser annealing have very many advantages in the modification of surfaces without altering the bulk characteristics. Some of the recent experiments show that all these techniques are highly non-equilibrium in nature and have characteristic time scales of the order of $10^{-10} - 10^{-13}$ sec. Thus, these methods can yield exotic and novel metastable phases and stable compositions in which limits of solid solubility and Hume Rothery rules are relaxed considerably.

In the characterization of surface layers and interfaces, Conversion Electron Mössbauer Spectroscopy has a number of advantages. The technique not only helps in characterizing the surface layers and bringing out details of interface reactions, but also helps in elucidating the very process of the modification of surfaces. Besides, Conversion Electron Mössbauer Spectroscopy finds applications in the study of thin films, phenomena of catalysis and chemisorption as also in understanding of the atomic arrangements in glassy metals.

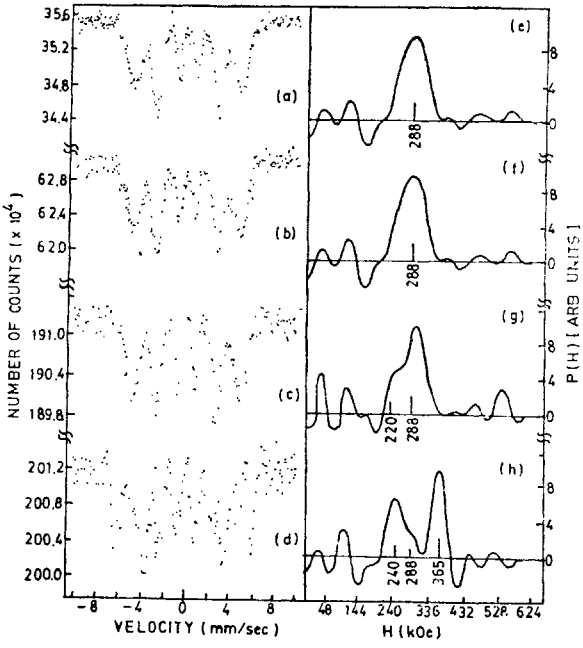

FIG. 5.4 Transmission Mössbauer spectra of as-received metglass (a), and metglass annealed at 300°C (b), 390°C (c), and 440°C (d); for ten hour each. The hyperfine field distributions [P(H) curves] corresponding to the transmission spectra in (a), (b), (c) and (d) are shown in (e), (f), (g) and (h) respectively.

ACKNOWLEDGEMENTS

The authors gratefully acknowledge the help and cooperation of the members of the 'Submicron-Physics Group' of the Department of Physics, University of Poona in carrying out the work which has been included in the present article as the contribution of the 'Poona Group'. These members include Dr S. M. Chaudhari, Mr. V. P. Godbole, Mr. S. A. Kulkarni, Mr. Y. S. Dorik, Mrs. Rekha Joshee, Mr. P. P. Patil, Mr. Y. V. Bhandarkar, Mr. D. M. Phase, Mrs. Jayashree Patankar and Mr. D. B. Shinde. Three of us (SBO, SVG, SMK) are also thankful to Professor M. R. Bhiday. Professor A. S. Nigavekar, Professor P. S. Damle and Dr. V. N. Bhoraskar for their help and encouragement and for making the appropriate Institutional facilities available to us.

The research programmes undertaken by the 'Submicron Physics Group' in the field of 'radiation processing of surfaces interfaces and thin films' have been funded by the Department of Science and Technology (DST) Defence Research and Development Organisation (DRDO), Department of electronics (DOE), Department of Atomic Energy (DAE) and Counil of Scientific and Industrial Research (CSIR), India. The authors gratefully acknowledge the support of these funding agencies.

The authors are also grateful to the scientists who have kindly permitted the reproduction of their results in the present article.

REFRENCES

1. *Surface Modification and Alloying by Laser,* Ion and Electron Beams, (Ed : J. M. Poate, G. Foti, D C Jacobson), Plenum Press, New York, London, 1981.
2. *Thin Films—Interdiffusion and Reactions,* (Ed : J M Poate, K N Tu, J W Mayer, A Wiley—Interscience Publication, New York, 1978).
3. *Laser and Electron Beam Solid interactions and Materials* Processing, (Ed : J F Gibbson, L D Hess, T W Sigmon, Elsevier North Holland, New York, 1981).
4. *Laser and Electron-beam Processing of Materials,* (Ed : C W White, PS Peercy, Academic Press, New York, 1980).
5. Duwez, Paul *J. Vac. Sci. Tech.*, **B1(2)**, (1983) 218.
6. J W, Erikson, L and Davies, J A *Ion implantation in Semiconductors,* Plenum Press, Mayer, New York, London, (1970).
7. Crowder B L (Ed) *Ion Implantation in Semiconductors and other materials,* Plenum Press, New York, London, (1973).
8. Carter, G and Colligon, J S (1968) *Ion bombardment of solids,* (Gresham Press, England.)
9. *Surface Modification and Alloying by Laser, Ion and Electron Beams,* (Ed : J M Poate, G Foti, D C Jacobson, Plenum Press, New York, London, 1981), Chapter 9.
10. Hoonhout, D Ph.D. Thesis, Fom Institute, The Netherlands (1981).
11. Sood, D K (1982) *Rad. Eff.*, **63**, 141.
12. Bhide, V G *Mössbauer Effect and its Applications,* Tata McGraw Hill Publishing Co. Ltd. New Delhi, (1973).
13. Gonser, U (Ed.) *Mössbauer Spectroscopy-II,* (Springer Verlag Berlin, Heidelberg, New York, (1981).
14. Jaggi, N K Ph.D. Thesis, Bombay University, Bombay, India, (1982).
15. *Surface Modification and Alloying by Laser, Ion and Electron Beams,* (Ed: J M Poate, G Foti, D C Jacobson, Plenum Press, New York, London, 1981), Chapter 7.

16. Sood, D K *Phys. Lett.* **68A,** (1978) 469.
17. Dearnaley, G *Nucl. Instr. and Meth.,* **182/183,** (1981) 899.
18. Tsaur, B Y, Liau, Z L and Mayer, J W *Appl. Phys. Lett.,* **A71,** (1979) 270.
19. Lau, S S, Tsaur, B Y, Von Allmen, M, Mayer, J W, Strizker, B, White, C W and Appleton, B *Nucl. Instr. and Meth.,* **182/183,** (1981) 97.
20. Tsaur, B Y and Hung L S *Appl. Phys. Lett.,* **37**(10), (1980) 922.
21. Hung, L S, Nastasi, M, Gyulai, J and Mayer, J W *Appl. Phys. Lett.,* **42**(8), (1983) 672.
22. Mazoldi, P, Dona, Dalle L F, Rose, and Sood, D K *Rad. Eff.,* **63,** (1982) 105.
23. Tsou, S C, Tsien, P H, Takai, M., Roschenthaler, D, Ramin, M, Ryssel, H and Ruge, I *Appl. Phys.,* **23,** (1980) 163.
24. Gat, A, Gerzberg, L, Gibbson, J F, Magee, T J, Peng, J and Hong, J D, *Appl. Phys. Lett.,* **33,** (1978) 775.
25. Bamchil, G, Bensahel, D, Goldanskii, A, Ferrieu, F, Auvert, G, Perio, A and Pfister, J C *Appl. Phys. Lett.,* **41**(1), (1982) 46.
26. Wang, J C, Wood, R F and Pronko, P P *Appl. Phys. Lett.,* **33,** (1978) 455.
27. Von, J A, Vechten, Tsu, R and Saris, F W *Phys. Lett.,* **A74**(6), (1979) 422.
28. Baeri, P, Compisano, S V, Foti, G and Rimini, E *Phys. Rev. Lett.,* **41,** (1978) 1246.
29. *Laser and Electron Beam Solid Interactions and Material Processing,* (Ed: J F Gibbsons, L D Hebs, T W Sigmon, Elsevier North Holland Inc. New York, 1981), pp. 45–47, 511–524.
30. Sawicka, B D and Sawicki, J A In *Mossbauer Spectroscopy-II,* (Ed: U Gonser, Springer Verlag Berlin, Heidelberg, New York), (1981) .
31. Hussey, R J, Coplan, D and Graham, M J *Oxidation of Metals,* **15**(5/6), (1981) 421.
32. Longworth, G and Hartley, N E W *Thin Solid Films,* **48**(1), (1978) 95.
33. Kanetkar, S M, Dorik, Y S, Chaudhari, S M, Ogale, S B and Bhide V G *Thin Solid Films* (Submitted).
34. Baumvol, I J R *J. Appl. Phys.,* **52**(7), (1981) 4583.
35. Dorik, Y S, Bhide, V G, Kanetkar, S M, Ghaisas, S V, Chaudhari, S M and Ogale, S B *J. Appl. Phys.* August 1984 issue, (in press).
36. Bayreuther, G *J. Vac. Sci. Tech.,* **A 1**(1), (1983) 19.
37. Mullen, J G and Stevenson, J *Nucl. Instr. and Meth.,* **153,** (1978) 77.
38. Tyliszczak, T, Sawicki, J A, Stanek, J, and Sawicka, B D *Journal de Physique,* **C-1,** (1980) 117.
39. Sprouse, G D, Kalvius, G M and Hanna, S S *Phys. Rev. Lett.,* **18,** (1965) 1041.
40. Sawicka, B D, Drwiega, M, Sawicki, J A and Stanek, J *Hyperfine Interactions,* **5,** (1978) 147.
41. Nasu, S, Gonser, U and Preston, R S *Journal de Physique,* **C-1,** (1980) 385.
42. Sawicka, B D and Sawicki, J A *Phys. Lett.,* **A64,** (1977) 311.
43. Sawicki, J A and Sawicka, B D *Phys. Stat. Sol.*' **B88,** (1977) K 41.
44. Jastrzebski, Z D *The Nature and properties of Engineering materials,* (John Wiley and Sons, Inc. New York, U.S.A.), (1976).
45. Godbole, V P, Bhide, V G, Ghaisas, S V, Kanetkar, S M, Chaudhari, S M and Ogale, S B (1984) *Mat. Res. Soc. Symp.* Proc. (Thin Films and Interfaces-II, Eds. Baglin, Campbell, Chu; Elsevier Science Publishing Co. Inc.), **25,** 247.
46. Godbole, V P, Bhide, V G, Ghaisas, S V, Kanetkar, S M, Joshee, R S and Ogale, S B (1984) *Mat. Res. Soc. Symp. Proc.* (Thin Films and Interfaces-II, Eds. Baglin, Compbell, Chu; Elsevier Science Publishing Co. Inc.), **25.**
47. Godbole, V P, Chaudhari, S M, Ghaisas, S V, Kanetkar, S M, Ogale, S B and Bhide, V G *Phys. Rev.* **B** (Submitted).
48. Ogale, S B, Joshee, Rekha, Godbole, V P, Kanetkar, S M and Bhide, V G *J. Appl. Phys.* (U.S.A) (in Press).
49. Patankar, Jayashree, Bhandarkar, Y V, Kanetkar, S M, Ogale, S B and Bhide, V G, *Nucl. Instr. and Meth.* (in Press).
50. Ogale, S B, Godbole, V P, Kanetkar, S M and Bhide, V G *Appl. Phys. Lett.* (Submitted).

51. Preston, R S (1972) *Met. Trans.*, **3**, 1831.
52. Hirvonen, H and Raisanen J *J. Appl. Phys.*, **53**(4), (1982) 3314.
53. Gonser, U and Ron, M In *Applications of Mössbauer Spectroscopy* ol. II, ((Ed: R L Cohen, Academic Press, New York, 1980).
54. Terrell, J H and Spijkerman, J J *Appl. Phys. Lett.*, **13**, (1968) 11.
77. O'Grady, W E *J. Electrochem. Soc.*, **127**, (1980) 555.
56. Eldridge, J, Kordesch, M E and Hoffman, R W *J. Vac. Sci. Tech.*, **20**, (1982) 934.
57. Kundig, W, Bommel, H, Constabaris, G and Lindquist, R H *Phys. Rev.*, **142**, (1966). 327.
58. Petrikin, Yu V, Damgaard, S, Oron, M, Petersen J W and Weyer, G *Journal de Physique*, **C—11**, (1980) 423.
59. Blaauw, C, Woude, Van, der and Sawatzky, G A (1973) *J. Phy. C.* (*Solid State*), **6**, 2371.
60. Prasad, K G. *Proc. of the International Conference on the Applications of the Mössbauer Effect*, Jaipur, India (Dec. 1981).
61. Dektiyar, I Y, Nomoshkalenko, V V, Nishchenko, M M, Razumov, O N and Tomashevasky, N A (1983) *Proc. of International Conference on the Applications of the Mossbauer Effect* (Alma Ata, USSR).
62. Nasu, S and Gonser, U. *Journal de Physique. Coll.*, **B.20**, (1979) 476.
63. Ok, N H and Morrish, A H *Phy. Rev. B.*, **23**(5), (1981) 2257.
64. Ogale, S B, Bhandarkar, Y V, Patil, P P, Kanetkar, S M and Bhide, V G *Phy. Rev. B.* (Submitted).
65. Johnson, C E, Ridout, M S and Cranshow, T E (1963) *Proc. Phys. Soc.*, **81**, 1079.
66. Ok, H N and Morrish, H *Phy. Rev. B.*, **22**(7), (1980) 3471.
67. Gupta, D, Tu, K N and Asai, K W *Phy. Rev. Lett.*, **35**(12), (1975) 796.